

Amplitude Equations for Reaction-Diffusion Systems with a Hopf Bifurcation and Slow Real Modes

M. Ipsen[†] F. Hynne[‡] P. G. Sørensen[‡]

October 28, 2018

Abstract

Using a normal form approach described in a previous paper we derive an amplitude equation for a reaction-diffusion system with a Hopf bifurcation coupled to one or more slow real eigenmodes. The new equation is useful even for systems where the actual bifurcation underlying the description cannot be realized, which is typical of chemical systems. For a fold-Hopf bifurcation, the equation successfully handles actual chemical reactions where the complex Ginzburg-Landau equation fails. For a realistic chemical model of the Belousov-Zhabotinsky reaction, we compare solutions to the reaction-diffusion equation with the approximations by the complex Ginzburg-Landau equation and the new distributed fold-Hopf equation.

Keywords: Nonlinear dynamical systems and chemical waves; bifurcation theory; amplitude equations.

PACS: 05.45.-a; 87.18.Pj; 47.20.Ky;

[†]UNI•C, Danish Computing Center for Research and Education, The Technical University of Denmark, Building 304, DK-2800 Lyngby, Denmark, (corresponding author, email: mads.ipsen@uni-c.dk).

[‡]Department of Chemistry, University of Copenhagen, H.C.Ørsted Institute, Universitetsparken 5, DK-2100 Copenhagen, Denmark.

1 Introduction

Near a bifurcation, the evolution of a dynamical system exhibits critical slowing down, which often admits a simplified description in terms of an amplitude equation. We demonstrate in this paper that slow modes may sometimes be described in terms of amplitude equations even if the underlying bifurcation cannot be realized for a given system. More specifically, we show that slow modes additional to the critical modes of a bifurcation may be treated in terms of a higher-codimension bifurcation.

Near a Hopf bifurcation, a reaction-diffusion system may sometimes be described by a complex Ginzburg-Landau equation (CGLE¹), where the motion is restricted to the unfolded center manifold of the focus. Diffusion may tend to move the system off that slow manifold, but fast non-oscillatory modes may keep the state point close to it. However, if the system has a slow real mode, diffusion may significantly excite that mode, thus making a description in terms of the CGLE dubious.

In principle, a system with a Hopf bifurcation and a slow real mode may always be treated by a CGLE provided we work sufficiently close to the bifurcation point. But experimental limitations may prevent us from operating close enough. Slow modes are likely to appear in complex chemical or biochemical reactions where the spectrum of characteristic times often spans many orders of magnitude. An example is the Belousov-Zhabotinsky (BZ) reaction which under certain conditions shows simple periodic oscillations. These basic oscillations may be described by relatively simple models like the Oregonator [1]. At other operating points, the BZ reaction may exhibit complex oscillations (including chaos) [2, 3], which can be attributed to the presence of a slow real mode and cannot be described by the Oregonator. But the complexity of the BZ reaction can be described quite well by a four-dimensional extension of the Oregonator model [3]. For that more realistic model, we show in this paper that a description by the CGLE fails at experimentally feasible conditions.

Treating a reaction-diffusion system by an amplitude equation saves computational resources and provides interpretations that give more insight into the character of the solution. It is therefore highly desirable to develop an amplitude description to replace the CGLE for important chemical systems like the BZ reaction or biochemical reactions such as glycolysis. In this paper, we shall derive an amplitude equation for reaction-diffusion systems with a Hopf bifurcation and a slow real mode. The equation is based on the amplitude equation for a fold-Hopf bifurcation even though the system need not possess such codimension-two bifurcation. We shall refer to the result as a distributed slow-Hopf equation (DSHE). We show that the four-dimensional reaction-diffusion model of the BZ reaction may be excellently described in terms of the appropriate DSHE.

The development of the DSHE involves several intermediate results that are important in their own right. We first derive a set of amplitude equations for the class of bifurcations (occurring in the corresponding spatially homogeneous system) with one pair of pure imaginary eigenvalues and any number of semisimple eigenvalues zero. (Chemical and biochemical reactions may well have several slow modes.)

The method used for deriving the amplitude equations builds on results previously obtained for ordinary differential equations [4]. The unfolded center manifold for the corresponding homogeneous system is parameterized by points \mathbf{y} in the center subspace. At each point of (physical) space, the state point is restrained to move on the center manifold, and the amplitude equation is found as the equation for the modulation of the oscillations of \mathbf{y} (described in a basis of critical eigenvectors) obtained from the restrained reaction-diffusion equation.

¹In this paper, we use the following abbreviations: CGLE: “Complex Ginzburg-Landau equation”; DSHE: “Distributed slow-Hopf equation”; BZ: “Belousov-Zhabotinsky”.

The resulting class of amplitude equations for the general case is given by Eq. (19) with Eqs. (20) and (21). From a solution to an amplitude equation, we get the physical solution using the transformation (22), determined as indicated in Appendix A (see also [4]).

We treat the special case of a distributed fold-Hopf bifurcation in detail in Section 2.3 (see Eq. (24) together with Table 1). We note also that the CGLE is another special case; thus the present work contains a new derivation of that important equation.

We modify the distributed fold Hopf equation to get an amplitude equation, the DSHE, applicable to systems with a Hopf bifurcation and one slow but non-critical real mode. The result is Eq. (27), which can be scaled to the dimensionless form Eq. (31). The precise relation of the DSHE to the original CGLE is required when the two equations are compared. It is explained in Appendix C.

The approximations in terms of various amplitude equations are evaluated for a four-dimensional extension of the Oregonator model mentioned above, which is described in Section 4.1. The model provides a realistic description of the BZ reaction based on extensive kinetic work [5, 6] and describes much of the dynamical behavior of the BZ system qualitatively or semiquantitatively correctly (see [3] for a description of the complex dynamics and [7] for the bare oscillations).

We compare the “exact” solution obtained by direct numerical integration of the reaction-diffusion equation with the approximations obtained as solutions to the amplitude equations, the CGLE on the one hand and the DSHE on the other. We find in Sections 4.3 and 4.4 that whereas the simple CGLE fails, the DSHE provides a very accurate description of the dynamics of the reaction-diffusion system.

The result shows the effect of a slow real mode near a Hopf bifurcation, and that a Ginzburg-Landau approximation cannot be considered reliable for the BZ system. The slow real mode is a natural (unavoidable) part of that system. A similar effect has also been considered by Aranson et. al [8] who coupled the FitzHugh-Nagumo model [9, 10] with an artificial slow real mode. There the slow mode interacted with an excitable system, and the effect was the opposite of the one reported here for the oscillatory BZ system. Random initial conditions normally give rise to a disordered distribution of spiral waves in the FitzHugh-Nagumo model, but the slow mode resulted in the development of a single spiral covering the entire spatial domain.

2 Derivation of amplitude equations

In this section, we derive amplitude equations for chemical reaction-diffusion systems for which the (spatially) homogeneous system is near a bifurcation at which the spectrum of critical eigenvalues consists of one pair of complex conjugate, imaginary eigenvalues and several real semisimple eigenvalues equal to zero.

2.1 Homogeneous systems

We consider a dynamical system, described by a vector $\mathbf{x} \in \mathbb{R}^n$, and depending on a set of parameters $\boldsymbol{\mu} \in \mathbb{R}^s$. The system is supposed to have a stationary point $\mathbf{x}_s(\boldsymbol{\mu})$ at which a local bifurcation occurs at $\boldsymbol{\mu} = \mathbf{0}$. We shall use the stationary point, $\mathbf{x}_s(\mathbf{0})$, at the bifurcation point as origin. The homogeneous chemical system evolves according to the kinetic equation

$$\frac{d\mathbf{x}}{dt} = \mathbf{F}(\mathbf{x}; \boldsymbol{\mu}) = \mathbf{J} \cdot \mathbf{x} + \mathbf{f}(\mathbf{x}, \boldsymbol{\mu}). \quad (1)$$

The Jacobian matrix at the stationary point at the bifurcation, $\mathbf{J} = D\mathbf{F}(\mathbf{0}, \mathbf{0})$, has r semisimple eigenvalues λ_i and r pairs of linearly independent right and left eigenvectors \mathbf{u}_i and \mathbf{u}_i^* , normalized according to the biorthonormality relations

$$\mathbf{u}_i^* \cdot \mathbf{u}_j = \delta_{ij}, \quad \text{for } i, j = 1, \dots, r. \quad (2)$$

The r -dimensional center manifold W^c at $\boldsymbol{\mu} = \mathbf{0}$ is tangent to the center subspace E^c at $\mathbf{x} = \mathbf{0}$, which is spanned by the r right eigenvectors \mathbf{u}_i . Near $\mathbf{x} = \mathbf{0}$, motion in W^c (or its unfolding) is usually much slower than motion towards it or away from it (critical slowing down), and the motion outside W^c may often be considered transient and fast and therefore disregarded. This fact adds to the practical importance of the center manifold.

We have previously [4] derived simple, explicit expressions that allow us to write down the normal form equation for the flow on the center manifold and unfoldings of it (for $\boldsymbol{\mu} \neq \mathbf{0}$) as well as a transformation from normal form coordinates to the original physical coordinates. The transformation has the form of a map

$$\mathbf{x} = \mathbf{y} + \mathbf{h}(\mathbf{y}, \boldsymbol{\mu}), \quad \text{where } \mathbf{y} \in E^c, \quad (3)$$

from $E^c \times \mathbb{R}^s$ to the (unfolded) center manifold. For oscillatory modes, the normal form allows a formulation in terms of “amplitudes” by a straightforward modification of the normal form equation. Consequently, we sometimes refer to the equation as an “amplitude equation”, whether it is modified or not. The results of the previous work needed in the present paper are summarized in Appendix A.

From the results of Appendix A, we may easily obtain an explicit expression for the center manifold, parameterized by coordinates in the center subspace in a basis of critical eigenvectors, valid for any given local bifurcation (with semisimple critical eigenvalues). We refer to such representation as an “amplitude transformation”. It is given by Eq. (3) with \mathbf{h} expanded in powers of the coordinates of \mathbf{y} , see Eq. (44) of Appendix A. Observe that this expansion also provides an explicit expression for the vector field on W^c . We shall make use of these two results in the next subsection to derive an amplitude equation for the corresponding reaction-diffusion problem.

2.2 Extension to spatially inhomogeneous systems

When the system described by Eq. (1) is modified by introducing diffusion of the involved physical quantities, the time evolution of the system is governed by a reaction-diffusion equation

$$\frac{\partial \mathbf{x}}{\partial t} = \mathbf{F}(\mathbf{x}; \boldsymbol{\mu}) + \mathbf{D} \cdot \nabla^2 \mathbf{x}, \quad (4)$$

where $\mathbf{x} = \mathbf{x}(\mathbf{r}, t)$ depends on a spatial position \mathbf{r} as well as time t , and \mathbf{D} is a diffusion operator, which typically, to a good approximation, can be represented by a diagonal matrix.

In a homogeneous system, the (unfolded) center manifold is invariant under the flow. In chemical reaction-diffusion systems, diffusion may take the local concentration away from W^c even if it initially was on W^c everywhere.

However, close to the bifurcation, the motion on the unfolded center manifold due to the chemical reactions often is much slower than motion transverse to it, as already mentioned. Consequently, diffusion never takes the system far away from that “slow manifold”, so the evolution of the spatial system may be approximately described by Eq. (4) with \mathbf{x} restrained to move on the slow manifold $W^c(\boldsymbol{\mu})$ given by Eq. (3).

We may therefore simply substitute the right hand side of Eq. (3) for \mathbf{x} in Eq. (4) to get a differential equation in \mathbf{y} , the corresponding point in the center subspace. The appropriate solution to the resulting equation is then transformed by Eq. (3) to the motion in the center manifold, the approximate solution to the reaction-diffusion equation (4).

Unfortunately, direct substitution of the parameterization for the slow manifold $W^c(\boldsymbol{\mu})$ in Eq. (4) results in “counter-rotating terms” [11] that prevent straightforward use of amplitudes for oscillatory modes. By averaging, these recalcitrant terms can be seen to be negligible close enough to the bifurcation point, but that method is approximate and inelegant. We shall therefore use a method of two times while still building on the result of the theory outlined in Appendix A.

We now restrict the discussion to a bifurcation with a single pair of complex conjugate imaginary eigenvalues $\pm i\omega_0$ together with any number of semisimple zero eigenvalues. There are r such critical eigenvalues (counting multiplicity) and r linearly independent right eigenvectors and corresponding left eigenvectors satisfying the biorthonormality relations (2). The period of the oscillations near $\mathbf{x} = \mathbf{0}$ at $\boldsymbol{\mu} = \mathbf{0}$ is $T = 2\pi/\omega_0$.

We express the solution $\mathbf{y}(\mathbf{r}, t)$ as the modulation of harmonic oscillations of frequency ω_0 for the oscillatory mode and seek an equation for the modulation. To that end, it is convenient to view \mathbf{y} as a function of two independent time variables, τ and θ , with θ accounting for the harmonic oscillation (of the oscillatory degrees of freedom) and τ describing the modulation.

We define

$$\mathbf{y}(\mathbf{r}, \tau, \theta) = e^{\mathbf{J}\theta} \cdot \mathbf{z}(\mathbf{r}, \tau) = \sum_{i=1}^r e^{\lambda_i \theta} z_i(\mathbf{r}, \tau) \mathbf{u}_i, \quad (5)$$

where τ and θ are given functions of time. At the end of the calculation, we shall choose

$$\tau = \theta = t. \quad (6)$$

To obtain the correct equation for $\mathbf{y}(\mathbf{r}, \tau, \theta)$, we use Eq. (6) initially as

$$\frac{\partial \mathbf{y}}{\partial t} = \frac{\partial \mathbf{y}}{\partial \theta} \frac{d\theta}{dt} + \frac{\partial \mathbf{y}}{\partial \tau} \frac{d\tau}{dt} = \frac{\partial \mathbf{y}}{\partial \theta} + \frac{\partial \mathbf{y}}{\partial \tau}. \quad (7)$$

but otherwise we use the variables \mathbf{r} , τ , and θ consistently throughout (so no confusion should arise from using the symbol \mathbf{y} for the two different functional forms).

We now view \mathbf{x} as a function of \mathbf{r} , τ , and θ through Eq. (3), and using Eq. (7), the reaction-diffusion equation (4) may then be written as

$$\frac{\partial \mathbf{x}}{\partial \tau} = (\mathbf{J} \cdot \mathbf{x} - \frac{\partial \mathbf{x}}{\partial \theta}) + \mathbf{f}(\mathbf{x}, \boldsymbol{\mu}) + \mathbf{D} \cdot \nabla^2 \mathbf{x}, \quad (8)$$

with

$$\mathbf{x}(\mathbf{r}, \tau, \theta) = \mathbf{y}(\mathbf{r}, \tau, \theta) + \mathbf{h}(\mathbf{y}(\mathbf{r}, \tau, \theta), \boldsymbol{\mu}). \quad (9)$$

For a given physical (or chemical) problem, the transformation \mathbf{h} is a well defined function of \mathbf{y} and $\boldsymbol{\mu}$. So for a given $\boldsymbol{\mu}$, the second term of Eq. (9) and its derivatives with respect to \mathbf{r} , τ , and θ are completely determined by the function $\mathbf{y}(\mathbf{r}, \tau, \theta)$. Consequently, these terms do not contain any “new” information about the dynamics not already contained in $\mathbf{y}(\mathbf{r}, \tau, \theta)$ and the transformation $\mathbf{h}(\mathbf{y}, \boldsymbol{\mu})$.

These remarks suggest that we try to eliminate as much as possible of the nonlinear term of

$$\frac{\partial \mathbf{x}}{\partial \tau} = \frac{\partial \mathbf{y}}{\partial \tau} + \frac{\partial \mathbf{h}}{\partial \tau} \quad (10)$$

in Eq. (8). We observe that

$$\frac{\partial \mathbf{y}}{\partial \tau} = e^{\mathbf{J}\theta} \cdot \frac{\partial \mathbf{z}}{\partial \tau} = \sum_{i=1}^r e^{\lambda_i \theta} \frac{\partial z_i}{\partial \tau} \mathbf{u}_i \quad (11)$$

implying that we may extract an equation for $\frac{\partial z_i}{\partial \tau}$ by multiplying Eq. (8) by $e^{-\lambda_i \theta} \mathbf{u}_i^*$ (from the left) and averaging the result over a period T of θ . The left-hand side of Eq. (8) then simply gives $\frac{\partial z_i}{\partial \tau}$, since

$$\frac{1}{T} \int_0^T e^{-\lambda_i \theta} \mathbf{u}_i^* \cdot \frac{\partial \mathbf{h}}{\partial \tau} d\theta = 0. \quad (12)$$

We prove this property in Appendix B. There we also show that

$$\frac{1}{T} \int_0^T e^{-\lambda_i \theta} \mathbf{u}_i^* \cdot (\mathbf{J} \cdot \mathbf{x} - \frac{\partial \mathbf{x}}{\partial \theta}) d\theta = 0, \quad (13)$$

implying that the two terms in parentheses disappear from Eq. (8) by the above operation.

As argued in Appendix A, we may use a power series expansions of \mathbf{x} and $\mathbf{f}(\mathbf{x}, \boldsymbol{\mu})$ for \mathbf{x} on the slow manifold $W^c(\boldsymbol{\mu})$. Here we first note that

$$\mathbf{y}^{\mathbf{p}} = \prod_i y_i^{p_i} = \exp(\sum_i p_i \lambda_i \theta) \prod_i z_i^{p_i} = e^{\mathbf{p} \cdot \boldsymbol{\lambda} \theta} \mathbf{z}^{\mathbf{p}} \quad (14)$$

in concise notation.

For $\mathbf{f}(\mathbf{x}, \boldsymbol{\mu})$, we get using the expansion (49)

$$\begin{aligned} \frac{1}{T} \int_0^T e^{-\lambda_i \theta} \mathbf{u}_i^* \cdot \mathbf{f}(\mathbf{y} + \mathbf{h}(\mathbf{y}, \boldsymbol{\mu})) d\theta &= \frac{1}{T} \sum_{\mathbf{p}\mathbf{q}} \mathbf{u}_i^* \cdot \mathbf{f}_{\mathbf{p}\mathbf{q}} \mathbf{z}^{\mathbf{p}} \boldsymbol{\mu}^{\mathbf{q}} \int_0^T e^{(\mathbf{p} \cdot \boldsymbol{\lambda} - \lambda_i) \theta} d\theta \\ &= \sum_{\mathbf{p}\mathbf{q}}^i f_{\mathbf{p}\mathbf{q}}^{(i)} \mathbf{z}^{\mathbf{p}} \boldsymbol{\mu}^{\mathbf{q}}, \end{aligned} \quad (15)$$

in which $f_{\mathbf{p}\mathbf{q}}^{(i)} = \mathbf{u}_i^* \cdot \mathbf{f}_{\mathbf{p}\mathbf{q}}$ is the i 'th component of the vector coefficient of the expansion of $\mathbf{f}(\mathbf{x}, \boldsymbol{\mu})$ on $W^c(\boldsymbol{\mu})$ whereas the sum is taken over all sets (\mathbf{p}, \mathbf{q}) for which the resonance condition for the i 'th component

$$\mathbf{p} \cdot \boldsymbol{\lambda} = \sum_j p_j \lambda_j = \lambda_i \quad (16)$$

is satisfied. All other terms vanish because of the integral of the exponential in Eq. (15). Note that critical eigenvalues are either pure imaginary or zero. For clarity, the summation over the resonant terms for the i 'th component is marked with a superscript i in the sum in Eq. (15). For the diffusion term of Eq. (8), we similarly get (using the expansion (44) from Appendix A)

$$\begin{aligned} \frac{1}{T} \int_0^T e^{-\lambda_i \theta} \mathbf{u}_i^* \cdot \mathbf{D} \cdot \nabla^2 (\mathbf{y} + \mathbf{h}(\mathbf{y}, \boldsymbol{\mu})) d\theta &= \\ \sum_j D_{ij} \nabla^2 z_j \sum_{\mathbf{p}\mathbf{q}} \frac{1}{T} \int_0^T e^{(\lambda_j - \lambda_i) \theta} d\theta + \mathbf{u}_i^* \cdot \mathbf{D} \cdot \sum_{\mathbf{p}\mathbf{q}} \mathbf{h}_{\mathbf{p}\mathbf{q}} \boldsymbol{\mu}^{\mathbf{q}} \nabla^2 \mathbf{z}^{\mathbf{p}} \int_0^T e^{(\mathbf{p} \cdot \boldsymbol{\lambda} - \lambda_i) \theta} d\theta &= \\ \sum_j D_{ij} \nabla^2 z_j + \sum_{\mathbf{p}\mathbf{q}}^i \mathbf{u}_i^* \cdot \mathbf{D} \cdot \mathbf{h}_{\mathbf{p}\mathbf{q}} \boldsymbol{\mu}^{\mathbf{q}} \nabla^2 \mathbf{z}^{\mathbf{p}}. \end{aligned} \quad (17)$$

Here

$$D_{ij} = \mathbf{u}_i^* \cdot \mathbf{D} \cdot \mathbf{u}_j \quad (18)$$

and the sum over j is taken over all terms for which $\lambda_j = \lambda_i$, and the sum over \mathbf{p} and \mathbf{q} includes all resonant terms for the i 'th component (and no other). By using Eq. (12), Eq. (13), Eq. (15), and Eq. (17), we obtain an amplitude equation for the modulation as a set of coupled equations for the set of all coefficients $z_i(\mathbf{r}, \tau)$ defined in Eq. (5).

$$\frac{\partial z_i}{\partial t} = \sum_{\mathbf{p}\mathbf{q}}^i \mathbf{f}_{\mathbf{p}\mathbf{q}} \mathbf{z}^{\mathbf{p}} \boldsymbol{\mu}^{\mathbf{q}} + \sum_j d_{ij} \nabla^2 z_j + \sum_{\mathbf{p}}^i \mathcal{D}_{\mathbf{p}}^{(i)} \nabla^2 \mathbf{z}^{\mathbf{p}}. \quad (19)$$

Here

$$d_{ij} = \begin{cases} \mathbf{u}_i^* \cdot \mathbf{D} \cdot (\mathbf{u}_j + \sum_{|\mathbf{q}|>0} \mathbf{h}_{\delta_j \mathbf{q}} \boldsymbol{\mu}^{\mathbf{q}}), & \lambda_j = \lambda_i \\ 0, & \lambda_j \neq \lambda_i \end{cases} \quad (20)$$

and

$$\mathcal{D}_{\mathbf{p}}^{(i)} = \begin{cases} \mathbf{u}_i^* \cdot \mathbf{D} \cdot \sum_{\mathbf{q}} \mathbf{h}_{\mathbf{p}\mathbf{q}} \boldsymbol{\mu}^{\mathbf{q}} & |\mathbf{p}| > 1 \\ 0, & |\mathbf{p}| \leq 1, \end{cases} \quad (21)$$

in which $|\mathbf{p}| = \sum_j p_j$. As before, a superscript i restricts a summation to resonant terms for the i 'th component. In Eq. (20), the index set δ_j has components described by the usual Kronecker delta, $(\delta_j)_k = \delta_{jk}$.

In Eq. (19), we have identified τ with the “real” time, t , since we no longer need to distinguish between the two “formal” time scales. From a solution $z_i(\mathbf{r}, t)$, $i = 1, \dots, r$, to Eq. (19) we get an (approximate) solution to the reaction-diffusion equation (4) as

$$\mathbf{x}(\mathbf{r}, t) = \mathbf{y}(\mathbf{r}, t) + \mathbf{h}(\mathbf{y}(\mathbf{r}, t), \boldsymbol{\mu}), \quad (22a)$$

$$\mathbf{y}(\mathbf{r}, t) = \sum_{i=1}^r z_i(\mathbf{r}, t) e^{\lambda_i t} \mathbf{u}_i \quad (22b)$$

Here we note that the transformation \mathbf{h} produces anharmonic terms in θ in the plane of oscillations as well as components off the center subspace E^c . Of course, these terms are also modulated (by products of powers of the amplitudes z_i) and are therefore not periodic in t .

For a spatially homogeneous system, the diffusion terms disappear from the amplitude equation (19), and the result therefore agrees with the general expression for a homogeneous system as quoted in Appendix A. In general, the amplitude equation contains diffusion terms that modify the motion on the slow manifold. The sum over j in Eq. (19) represents the linear diffusion terms which include couplings between bifurcating modes corresponding to the same eigenvalue. But note in particular that the oscillatory modes (with eigenvalues $\pm i\omega_0$) do not couple to any of the real modes—only the real modes may couple to each other.

The nonlinear diffusion terms, the last sum in Eq. (19), arise because the motion is restrained to the slow manifold; diffusion is linear in \mathbf{x} but we describe the dynamics in terms of points $\mathbf{y} \in E^c$, and \mathbf{x} is clearly not linear in \mathbf{y} . It is to be expected, that the linear diffusion terms will dominate over the nonlinear diffusion, and these higher order terms may therefore be neglected in first approximation. Below we show examples which are excellently described using linear diffusion alone. In some cases, the nonlinear diffusion may be important, however. For example, this may be the case in situations where the real part of any of the

linear diffusion coefficients becomes negative—a situation which easily arises in biochemical systems where the diffusion constants may differ by several orders of magnitude.

In Section 2.3, we shall exhibit the amplitude equation for a fold-Hopf bifurcation (which has one oscillatory and one real mode) as a special case of Eq. (19). We also note how the well-known complex Ginzburg-Landau equation (CGLE) appears as a special case of the result (19). Thus the present work contains a novel derivation of the CGLE.

The fold-Hopf bifurcation will be used to solve the reaction-diffusion equation for a realistic model of the Belousov-Zhabotinsky reaction—we shall compare the solution obtained from the new equation with those of the reaction-diffusion equation itself and of the corresponding CGLE. In addition, this example also serves as an illustration of the practical use of Eq. (19).

2.3 Distributed Fold-Hopf equation

In the following, we shall focus on the special case of Eq. (19), where there is just a single eigenvalue in addition to the imaginary pair. This bifurcation is called a fold-Hopf bifurcation corresponding to the case where a Hopf bifurcation coincides with a single non-degenerate real bifurcation. The linear diffusion terms contain no coupling between modes, so the sum over j in Eq. (19) reduces to just one term, $d_{ii}\nabla^2 z_i$ with

$$d_{ii} = \mathbf{u}_i^* \cdot \mathbf{D} \cdot (\mathbf{u}_i + \sum_{\mathbf{q}} \mathbf{h}_{\delta_i, \mathbf{q}} \mu^{\mathbf{q}}). \quad (23)$$

Here we shall exhibit the amplitude equation (19) to lowest non-trivial order in μ (*i.e.* including only terms essential to the unfolding of local terms) implying that the diffusion term d_{ii} reduces to $d_{ii} = \mathbf{u}_i^* \cdot \mathbf{D} \cdot \mathbf{u}_i$.

To lowest order, we need only terms linear in μ in general, so we get similar independent terms from each component of μ . Therefore, we shall exhibit the result for a single scalar μ even though one is often interested in using two independent parameters for bifurcations of codimension two: the generalization is straightforward.

For convenience, we simplify the notation by assigning $\lambda_{1,2} = \pm i\omega_0$ and $\lambda_3 = 0$ for the eigenvalues at the bifurcation point, and $\mathbf{u}_1 = \mathbf{u}$, $\mathbf{u}_2 = \bar{\mathbf{u}}$, and $\mathbf{u}_3 = \mathbf{v}$ for the corresponding right eigenvectors. In this case, we need only consider the amplitudes for $w = z_1$ and $z = z_3$ since complex conjugation gives $z_2 = \bar{w}$.

If we include all terms up to third order in w and z for $q = 0$ and only terms essential to the unfolding for $q > 0$ and neglect nonlinear diffusion, we then obtain the following amplitude equation for a fold-Hopf bifurcation in a reaction-diffusion equation (4)

$$\dot{w} = \sigma_1 \mu w + g_0 w z + g_1 |w|^2 w + g_2 w z^2 + d_w \nabla^2 w, \quad (24a)$$

$$\dot{z} = \rho_0 \mu + c_0 |w|^2 + c_1 z^2 + c_2 |w|^2 z + c_3 z^3 + d_z \nabla^2 z. \quad (24b)$$

Here we have introduced the following compact notation

$$\begin{aligned} d_w &= \mathbf{u}^* \cdot \mathbf{D} \cdot \mathbf{u}, & d_z &= \mathbf{v}^* \cdot \mathbf{D} \cdot \mathbf{v}, \\ \sigma_1 &= \mathbf{u}^* \cdot \mathbf{f}_{1001}, & \rho_0 &= \mathbf{v}^* \cdot \mathbf{f}_{0001}, \\ g_0 &= \mathbf{u}^* \cdot \mathbf{f}_{1010}, & g_1 &= \mathbf{u}^* \cdot \mathbf{f}_{2100}, & g_2 &= \mathbf{u}^* \cdot \mathbf{f}_{1020}, \\ c_0 &= \mathbf{v}^* \cdot \mathbf{f}_{1100}, & c_1 &= \mathbf{v}^* \cdot \mathbf{f}_{0020}, & c_2 &= \mathbf{v}^* \cdot \mathbf{f}_{1110}, & c_3 &= \mathbf{v}^* \cdot \mathbf{f}_{0030}. \end{aligned} \quad (25)$$

The results derived for the fold-Hopf bifurcation are summarized in Table 1.

The amplitude equation for a reaction-diffusion system that undergoes a simple Hopf bifurcation is easily obtained from the general result Eq. (19) following the same procedure. As a result, we obtain the well-known complex Ginzburg-Landau equation (CGLE)

$$\dot{w} = \sigma_1 \mu w + g|w|^2 w + d \nabla^2 w. \quad (26)$$

The details of the results for the CGLE and explicit expressions for calculations of the coefficients in Eq. (26) are summarized in Table 2. The parameter d in Eq. (26) is identical with d_w , shown in Eq. (24).

3 Handling a slow noncritical mode

An amplitude equation very similar to the distributed fold-Hopf equation (24) can be derived for a system with a Hopf bifurcation and a slow real mode, even if only a Hopf bifurcation can be realized (near the desired operating point or anywhere at all). The result may be viewed as an extension of the complex Ginzburg-Landau equation.

3.1 The distributed slow-Hopf equation

We consider a system depending on a scalar parameter μ , having a Hopf bifurcation (for the homogeneous system) at $\mu = 0$. The critical eigenvalues are $\pm i\omega_0$ and the corresponding eigenvectors are \mathbf{u} and $\bar{\mathbf{u}}$. All other eigenvalues have negative real parts. One real eigenvalue is small, $|\lambda_0| \ll \omega_0$ (eigenvector \mathbf{v}) whereas all others satisfy $-\text{Re}\{\lambda\} \gg \omega_0$.

We may describe the system with a partial unfolding of the fold-Hopf equation, translated so that the origin is at the stationary point at $\mu = 0$. Unfolding of the Hopf bifurcation is governed explicitly by μ and needs no further discussion. The unfolding and translation from the fold-Hopf bifurcation to the particular Hopf bifurcation studied, can be accounted for by evaluating the fold-Hopf parameters at the Hopf bifurcation point, $(\mathbf{x}, \mu) = (\mathbf{0}, 0)$ instead of at the (fictitious) fold-Hopf point. In addition, the term $\rho_0 \mu$ of Eq. (19) disappears because of the translation to the new stationary point, and a term $\lambda_0 z$ appears explicitly, which was absent at the fold-Hopf bifurcation because λ_0 vanishes there. The relation of unfoldings to parameters of an amplitude equation and amplitude transformation, evaluated at a stationary point of an unfolded equation, has been discussed in section VII of [4].

The result of the modification is an equation of exactly the same form as Eq. (19) except that $\lambda_0 z$ replaces $\rho_0 \mu$. The coefficients are given by exactly the same formulas, Table 1, except that the Jacobian matrix and the other derivatives of the vector field are evaluated at the Hopf bifurcation point, and so are the eigenvalues and eigenvectors of \mathbf{J} . We shall refer to the equation as a distributed slow-Hopf equation (DSHE). Keeping the most important (lower order) terms only, the DSHE takes the form

$$\dot{w} = \sigma_1 \mu w + g_0 w z + g_1 |w|^2 w + d_w \nabla^2 w, \quad (27a)$$

$$\dot{z} = \lambda_0 z + c_0 |w|^2 + d_z \nabla^2 z, \quad (27b)$$

which we use in Section 4 to describe a realistic model of the BZ reaction-diffusion system.

The DSHE (27) is a generalization of the CGLE (26). It contains the simple CGLE as a special case when $|\lambda_0| \gg \text{Re}\{\sigma_1\}\mu$, as we show in Appendix C: there we discuss the relation between the two equations, and in particular we derive an explicit relation between the parameters g_1 and g . These parameters are in general quite different despite their deceptively similar definitions. The two amplitude equations are evaluated and compared numerically with each other and with the underlying reaction-diffusion equation in Section 4.

3.2 Scalings

Near a bifurcation, an evolution equation often scales with the bifurcation parameter(s) to lowest order(s) in a simple way. This property admits a reduction of the (truncated) equation to a form independent of the distance(s) from the bifurcation point. Examples of reduced equations are the Ginzburg-Landau equation [12], the Kuramoto-Sivashinsky equation [13, 14], and the Swift-Hohenberg equation [15].

For the fold-Hopf bifurcation, a complete scaling requires two carefully chosen bifurcation parameters. The DSHE (27) cannot be scaled to a form independent of the bifurcation parameter. Nevertheless, it is useful to introduce a partial rescaling of Eq. (27) with the substitutions

$$w = \sqrt{\mu}w', \quad z = \mu z', \quad t = t'/\mu, \quad \mathbf{r} = \mathbf{r}'/\sqrt{\mu} \quad (28)$$

to obtain an equation in the new, primed variables. If we drop the primes for simplicity, the scaled equation becomes

$$\dot{w} = \sigma_1 w + g_0 w z + g_1 |w|^2 w + d_w \nabla^2 w, \quad (29a)$$

$$\mu \dot{z} = \lambda_0 z + c_0 |w|^2 + \mu d_z \nabla^2 z. \quad (29b)$$

For analysis of solutions and numerical computations it is convenient to reduce Eq. (29) to dimensionless form by further scalings through the substitutions

$$w = \sqrt{\frac{-\sigma_1^r}{g_1^r}} w' \exp(i \frac{\sigma_1^i}{\sigma_1^r} t'), \quad z = \frac{\sigma_1^r}{g_0^r} z', \quad t = t'/\sigma_1^r, \quad \mathbf{r} = \sqrt{\frac{d_w^r}{\sigma_1^r}} \mathbf{r}', \quad (30)$$

in which superscripts r and i denote real and imaginary parts respectively. The result is an equation in the primed variables. If we skip the primes for convenience, the resulting rescaled equation takes the form

$$\dot{w} = w + (1 + i\gamma)wz - (1 + i\alpha_s)w|w|^2 + (1 + i\beta)\nabla^2 w, \quad (31a)$$

$$\epsilon \dot{z} = \lambda_0 z + \kappa |w|^2 + \epsilon \delta \nabla^2 z, \quad (31b)$$

where

$$\alpha_s = \frac{g_1^i}{g_1^r}, \quad \beta = \frac{d_w^i}{d_w^r}, \quad \gamma = \frac{g_0^i}{g_0^r}, \quad \epsilon = \mu \sigma_1^r, \quad \kappa = -c_0 \frac{g_0^r}{g_1^r}, \quad \delta = \frac{d_z}{d_w^r}. \quad (32)$$

The scalings used here are similar to those traditionally used for the CGLE [12] reducing it to the form

$$\dot{w} = w - (1 + i\alpha)w|w|^2 + (1 + i\beta)\nabla^2 w. \quad (33)$$

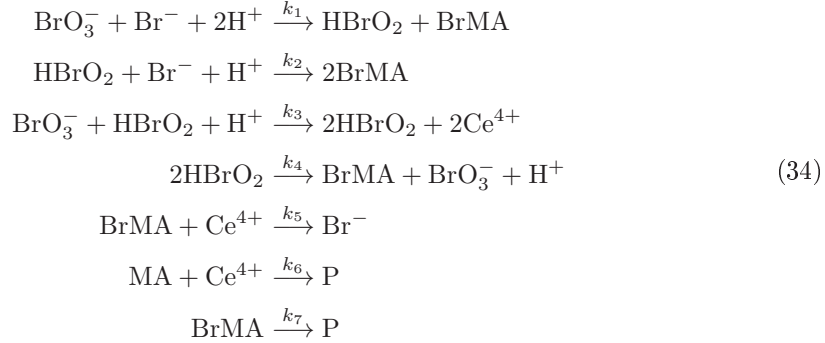
Here β is given by Eq. (32) and $\alpha = \frac{g_1^i}{g_1^r}$. The parameters α and α_s differ because g and g_1 do, as discussed further in Appendix C.

4 Comparison of solutions

The first successful attempt to model the oscillatory behavior of the BZ reaction was the Oregonator model suggested by Field and Noyes [1]. It exhibits both sinusoidal and relaxation oscillations in semi-quantitative agreement with many experiments. However, the Oregonator model does *not* reproduce more complex dynamics such as quasiperiodic oscillations or chaos.

4.1 Model of the BZ reaction

To incorporate complex phenomena of the BZ reaction into the modeling many different variants of the Oregonator have been considered. Here we use the modified Oregonator recently suggested by Wang et. al [3] to explain very complicated transient phenomena observed in the BZ reaction. The model, which we refer to as the 4D Oregonator, is based upon the following chemical scheme



Note that the first six reactions are equivalent with the reactions in the Oregonator model, except for the fact that bromomalonic acid (BrMA) appears explicitly in the scheme. The mechanistic assumption is that HBrO reacts immediately with malonic acid to produce BrMA. In order to explain the complexity observed in the closed system it is essential to add a reaction which corresponds to a removal of BrMA without a simultaneous production of Br^- . This additional feature is included in reaction 7 of Eq. (34).

Now, if we regard the concentration of BrMA as an additional dynamical variable and assume non-homogeneous spatial conditions, the above set of reactions gives rise to the following four-dimensional differential equation

$$\begin{aligned}
 \frac{\partial X}{\partial t} &= k_1 A H^2 Y - k_2 H X Y + k_3 A H X - 2k_4 X^2 + D_X \nabla_{\mathbf{r}}^2 X, \\
 \frac{\partial Y}{\partial t} &= -k_1 A H^2 Y - k_2 H X Y + k_5 U Z + D_Y \nabla_{\mathbf{r}}^2 Y, \\
 \frac{\partial Z}{\partial t} &= 2k_3 A H X - k_5 U Z - k_6 M Z + D_Z \nabla_{\mathbf{r}}^2 Z, \\
 \frac{\partial U}{\partial t} &= k_1 A H^2 Y + 2k_2 H X Y + k_4 X^2 - k_5 U Z - k_7 U + D_U \nabla_{\mathbf{r}}^2 U,
 \end{aligned} \tag{35}$$

where the following short-hand notation is introduced for the concentration of the chemical species: $X = [\text{HBrO}_2]$, $Y = [\text{Br}^-]$, $Z = [\text{Ce}^{4+}]$, $U = [\text{BrMA}]$, $A = [\text{BrO}_3^-]$, $H = [\text{H}^+]$, and $M = [\text{MA}]$. As in the Oregonator model, we regard A as a constant in order to study the system under open conditions. Besides having a supercritical Hopf bifurcation with small sinusoidal oscillations, the model also contains an additional slow time scale which primarily is related to the kinetics of BrMA. The values of the various constants in Eq. (35) are shown in Table 3.

4.2 Bifurcations and stability of waves

For the comparisons, we need to select a suitable operating point for the 4D Oregonator, close to a supercritical Hopf bifurcation. As parameters, we have chosen the fixed concentrations $[\text{BrO}_3^-]$ and $[\text{H}^+]$. All other parameters have been fixed using the values shown in Table 3.

The locus of Hopf bifurcations in the plane of the free parameters are shown in Fig. 1a. The bifurcation diagram consists of two apparently separate curves, which are connected for a very large and physically unrealistic value of $[\text{BrO}_3^-]$, however. Both branches describe supercritical Hopf bifurcations. The filled circle on the upper branch indicates a Hopf bifurcation point which has been chosen as reference point *viz.* $[\text{BrO}_3^-]_{\text{Hopf}} = 0.3662 \text{ M}$ and $[\text{H}^+]_{\text{Hopf}} = 1.3416 \text{ M}$. This reference point is characterized in Table 4. Since it is necessary to work at a non-zero distance from the bifurcation point, the actual operating point will be chosen close to this reference point. The variation of the Ginzburg-Landau parameters α and β , and the functional dependence $\beta(\alpha)$ are shown in Figs. 1b–1d. In all three cases, numbers ①–③ identify curves with the branches in the bifurcation diagram.

The reference point shown with a filled circle in Fig. 1 has been chosen with a view to the stability properties of waves. Reaction-diffusion equations may support several types of waves. Near a supercritical Hopf bifurcation, in particular, there may exist stable spiral waves as well as spatio-temporal chaos (chemical turbulence), depending on parameter conditions. Usually the CGLE approximation faithfully reproduce such behavior [16], and it is convenient to relate wave stability to the parameters, α and β , of the CGLE.

For the CGLE, the stability of spiral waves and their transitions to turbulent solutions in the α, β -parameter plane have been studied numerically and theoretically in [17, 18, 19]. One key observation in these studies is that the transition to turbulence in the CGLE is closely related to the concepts of convective and absolute instability. For spiral wave solutions, it was found that the boundary of the region for absolute instability is very close to the curve where spiral wave solutions exhibits a transition to turbulence. In addition, the region which separates the onset of convective instability of the spiral waves, to some extent, may be approximated by the Eckhaus instability border [18, 19]. The parameter space may therefore be divided into several subregions described by convective and absolute instabilities as in Fig. 1d. In the next section, we shall use these concepts in a discussion of suitable operating points to be selected for a comparison of the various equations, set up for the 4D Oregonator.

4.3 CGLE versus the reaction-diffusion equation

We choose the operating point well outside the region of absolute instability (AI in Fig. 1a) where we expect to observe stable spiral waves for the CGLE. Observe, that the chosen point lies close to the region of convective instability (EH), but this has no importance to the local stability properties of spiral waves. The Ginzburg-Landau parameters evaluated at the reference point are shown in Table 5.

The 4D Oregonator must be run at a non-zero distance from the Hopf bifurcation point. We choose the parameter values $[\text{BrO}_3^-] = 0.3625 \text{ M}$ and $[\text{H}^+] = [\text{H}^+]_{\text{Hopf}}$. This corresponds to an amplitude of the uniform oscillations, which is 7.5% of the stationary Ce^{4+} concentration. We emphasize that the CGLE is scaled and hence independent of the distance from the bifurcation point but the reverse scaling together with the amplitude transformation account for the distance actually used.

The most systematic way of comparing the solutions to the amplitude equation and the reaction-diffusion equation is to transform the space and time dependent complex amplitudes back to concentration space using the scalings described in Section 3.2 and the amplitude transformation determined in Table 2. The transformation is nonlinear, and the nonlinear terms are sometimes important [20].

For the present study, the linear part of the transformation

$$\mathbf{x}(\mathbf{r}, t; \mu) = \mathbf{x}_s(\mu) + \left[w(\mathbf{r}, t; \mu) e^{i\omega_0 t} \mathbf{u} + \text{c.c.} \right], \quad (36)$$

is sufficiently accurate. Equation (36) is expressed in terms of unscaled variables w , \mathbf{r} , and t . In addition, the unfolding terms describing the variation of the stationary point $\mathbf{x}_s(\mu)$ with the parameter μ are also incorporated. As an alternative to transforming amplitudes to physical variables for the comparison, one may calculate the amplitudes from the physical variables (concentrations) obtained from the reaction-diffusion equation. This is easy in the linear approximation to the amplitude transformation:

$$w(\mathbf{r}, t; \mu) = \mathbf{u}^* \cdot [\mathbf{x}(\mathbf{r}, t; \mu) - \mathbf{x}_s(\mu)] e^{-i\omega_0 t}. \quad (37)$$

The representation (37) is very convenient since the magnitude $|w|$ of the (unscaled) amplitude forms a very clear representation of an oscillatory wave.

In the comparisons, Figs. 2 and 3, we exhibit the magnitude $|w(\mathbf{r}, t; \mu)|$ as well as selected components of $\mathbf{x}(\mathbf{r}, t; \mu)$ (the concentrations of Ce^{4+} and BrMA) for solutions to the reaction-diffusion equation (RDE) and the CGLE respectively, using initial conditions suggested by Kuramoto [12] (we choose $|w(\mathbf{r}, t; \mu)|$ proportional to $|\mathbf{r}|$ and $\arg(w(\mathbf{r}, t; \mu)) = \arg(\mathbf{r})$, the polar angle).

As is clear from Fig. 3, the CGLE exhibits the behavior expected from the diagram Fig. 1d, a spiral wave solution evolving from the center of the grid. However, this very regular solution shows virtually no resemblance with that of the reaction-diffusion equation, Fig. 2. Focusing on $[\text{Ce}^{4+}]$, we see that a small spiral is initially formed at the center of the grid. After a few windings, the spiral is no longer able to maintain its structure, and a turbulent pattern develops. This is especially clear in the amplitude plot where a ‘‘shock wave’’ is emitted from the spiral core. When the shock hits the boundary of the domain, many small spirals are generated, the symmetry of the initial state breaks, and fully developed turbulence is reached. Here numerous small spirals are constantly created and annihilated, resulting in a disordered motion typical of chemical turbulence, which also has been observed in certain parameter regions for a reaction-diffusion equation based on the simple three dimensional Oregonator model [16].

4.4 DSHE versus the reaction-diffusion equation

The failure of the CGLE is clearly a result of the presence of a slow real mode in the 4D Oregonator, which violates a condition underlying a derivation of the equation: all motion towards the plane of the oscillations must be fast compared with the motion in the plane. We shall therefore try to describe the reaction-diffusion system with a distributed slow-Hopf equation, DSHE, which takes the slow real mode explicitly into account.

We work at the same operating point as used in the previous section so the results can be immediately compared with those for the CGLE and the reaction-diffusion equation. The parameters of the DSHE are evaluated at the Hopf bifurcation point using the formulas of Table 1. They are shown in Table 6. Note that the parameter g_1 is quite different from the corresponding CGLE coefficient g . This important difference is discussed in Appendix C.

We want to compare the solution to the DSHE with that of the reaction-diffusion equation first of all. For the latter, we might use Fig. 2, but to illuminate the role of the slow real mode, we shall calculate the real amplitude z as well as the concentrations of Ce^{4+} and BrMA.

The concentrations are obtained from the scaled amplitudes by reverse scaling and transformation back to concentration space with the amplitude transformation described in Table 1. As before, we consider only the linear part of the transformation here:

$$\mathbf{x}(\mathbf{r}, t; \mu) = \mathbf{x}_s(\mu) + (w(\mathbf{r}, t; \mu)e^{i\omega_0 t} \mathbf{u} + \text{c.c.}) + z(\mathbf{r}, t; \mu) \mathbf{v}, \quad (38)$$

(shown in terms of unscaled variables). In the linear approximation (38), we may alternatively calculate the amplitudes from a solution to the reaction-diffusion equation as

$$w(\mathbf{r}, t) = \mathbf{u}^* \cdot [\mathbf{x}(\mathbf{r}, t; \mu) - \mathbf{x}_s(\mu)] e^{-i\omega_0 t}, \quad (39a)$$

$$z(\mathbf{r}, t) = \mathbf{v}^* \cdot [\mathbf{x}(\mathbf{r}, t; \mu) - \mathbf{x}_s(\mu)]. \quad (39b)$$

The linear approximation (39a) to the complex amplitude w is identical to the one calculated for the CGLE, Eq. (37) (but the two amplitudes differ if nonlinear terms of the amplitude transformation are taken into account). Its magnitude $|w|$ has already been shown in Fig. 2, but to save space, we shall not exhibit $|w|$ for the DSHE. Instead, we show the real amplitude z together with $[\text{Ce}^{4+}]$ and $[\text{BrMA}]$ in Fig. 4 for the reaction-diffusion equation and Fig. 5 for the DSHE. Initial conditions for the simulations are the same as in the previous section [12].

The agreement between the two solutions is striking. Even quite subtle details agree for a long time although, eventually, the details of the turbulent patterns must disagree. However, the general character of the solutions continue to agree. Thus, the improvement of the DSHE-approximation over that of the CGLE, Fig. 3, is evident.

In conclusion, it is possible to treat a reaction-diffusion problem near a Hopf bifurcation using an efficient amplitude description, even for systems like the BZ-reaction that contain a very slow real mode as an intrinsic part of the chemistry. Essentially, the DSHE treats the Hopf bifurcation (of codimension one) as an unfolded fold-Hopf bifurcation of codimension two.

4.5 Role of the slow real mode

A conspicuous feature of the solutions to the reaction-diffusion equation, Fig. 4, or the DSHE, Fig. 5, is the similarity of the patterns for $[\text{BrMA}]$ and the amplitude z . In fact, the two patterns are almost identical either in Fig. 4 or in Fig. 5.

This similarity can be explained in terms of the eigenvectors of the Jacobian matrix whose numerical values, evaluated at the stationary point at the Hopf bifurcation, are shown in Table 7. We note that the eigenvector \mathbf{v} for the slow real mode is directed almost exactly along the $[\text{BrMA}]$ -axis.

Another noticeable feature of the solutions in Figs. 4 and 5 is the different characters of the components $[\text{BrMA}]$ and $[\text{Ce}^{4+}]$. Clearly, the spatio-temporal evolution of the BrMA pattern resembles that of $|w|$ much more (see Fig. 2). Again, the eigenvectors, Table 7, can throw some light on this feature. In the linear approximation, the left eigenvectors \mathbf{u}^* and $\bar{\mathbf{u}}^*$ (or the real and imaginary parts of \mathbf{u}^*) define the projection of any vector onto the plane of oscillation. From Table 7 we see that the $[\text{BrMA}]$ “component” of \mathbf{u}^* is very small compared with the other components of \mathbf{u}^* . This implies that $[\text{BrMA}]$ virtually does not participate in the basic oscillations of frequency ω_0 . Thus, apart from scale, the amplitude z can almost be identified with $[\text{BrMA}] - [\text{BrMA}]_0$.

To understand the behavior of $[\text{BrMA}]$ and the role of the amplitude z , we first watch the local variations of $\text{Re } w$ and z at an interior grid point from the simulation shown in Fig. 5. We observe that the amplitude R of the oscillations $\text{Re } w$ appear to vary in roughly the same way as z .

Setting $w = R \exp(i\Theta)$, gives the following differential equation for R and z in the homo-

geneous DSHE

$$\dot{R} = (\sigma_1^r + g_0^r z)R - g_1^r R^3, \quad (40a)$$

$$\mu \dot{z} = \lambda_0 z + c_0 R^2, \quad (40b)$$

where superscript r denotes the real part. To put Eq. (40) into dimensionless form we introduce the variable change

$$R = \sqrt{-\frac{\sigma_1^r}{g_1^r}} R', \quad z = \frac{\sigma_1^r}{g_0^r} z', \quad \text{and} \quad t = \frac{1}{\sigma_1^r} t'. \quad (41)$$

Skipping the primes for simplicity then gives the following dimensionless equation

$$\dot{R} = R + Rz - R^3, \quad (42a)$$

$$\dot{z} = \frac{\lambda_0 z + \kappa R^2}{\mu \sigma_1^r}, \quad \text{where} \quad \kappa = -c_0 \frac{g_0^r}{g_1^r}. \quad (42b)$$

Apart from $(0, 0)$, this scaled differential equation admits the non-trivial stationary solution

$$R_s = \left(1 + \frac{\kappa}{\lambda_0}\right)^{-\frac{1}{2}}, \quad z_s = -\frac{\kappa}{\kappa + \lambda_0}, \quad (43)$$

which corresponds to a uniform oscillatory solution to the reaction-diffusion equation. A numerical solution to Eq. (42) is shown in Fig. 7. Here, we observe that the point (R_s, z_s) corresponds to a stable focus in the (R, z) -plane—the trajectory exhibits a spiraling motion converging to the stationary state in agreement with the oscillatory modulation of the amplitude observed in Fig. 6. If we include diffusion into the description, this will serve as a constant perturbation, which keeps the solution away from the stationary solution (R_s, z_s) and thereby preserves the modulation of the amplitude. The interaction between the amplitudes R and z therefore introduces an additional frequency into the system, as observed in the torus-like behavior of the time series for $\text{Re } w$, and destroys the stability of spirals.

5 Conclusion

We have derived an amplitude equation that provides an efficient and accurate, approximate description of a reaction-diffusion system near a fold-Hopf bifurcation, as well as generalizations to systems with several critical real modes. The derivation is based on a normal form transformation combined with the use of two distinct time variables to handle slow modulations of oscillations. It does not rely on different time scales.

The derivation exhibits a simple geometrical interpretation of the amplitude equation in terms of the center manifold and center subspace, and it provides an explicit relation, the amplitude transformation, between amplitudes and physical variables. An amplitude equation is obtained as a truncation of a form containing infinite series, and there is a choice of including more or less terms. Similarly one may include more or less terms in the amplitude transformation. Observe that all coefficients can be calculated from the results of the theory.

The main result of the paper is the general amplitude equation Eq. (19) for a Hopf bifurcation and any number of “semisimple” critical real modes. It contains all the higher order terms mentioned, and in practice, it must be suitably truncated for any particular use. We note in particular that Eq. (19) includes nonlinear diffusion terms.

The special case of a fold-Hopf bifurcation is treated more explicitly in Section 2.3. Here the amplitude equation (24) is a selected truncation of Eq. (19) for the case of a single real critical mode. The coefficients (25) are given explicitly by Table 1 in terms of coefficients $\mathbf{h}_{\mathbf{p}\mathbf{q}}$ obtained by solving the linear equations shown.

The fold-Hopf bifurcation has codimension two, and we would not expect to find a realization of this bifurcation in any particular reaction-diffusion system. Nevertheless, we show that a description based on the dynamics of a fold-Hopf bifurcation is much more versatile than the codimension initially suggests.

We show that the machinery used to derive the distributed fold-Hopf equation (24) can be used to derive what we have called the distributed slow-Hopf equation (27), the DSHE, applicable to a reaction-diffusion system with a simple Hopf bifurcation together with a slow (near-critical) real mode. The DSHE (27) differs from the general amplitude equation (19) by including the linear term $\lambda_0 z$ which is absent at criticality. In addition, all its coefficients are evaluated at the Hopf bifurcation. It includes terms sufficient for the particular reaction-diffusion problem discussed: a four-dimensional model of the Belousov-Zhabotinsky (BZ) reaction exhibited in Section 4.1, the 4D Oregonator.

The purpose of looking at the 4D Oregonator (35) is first of all to test the DSHE by comparing solutions to it with solutions to the reaction-diffusion equation and to the corresponding CGLE, all computed at the same operating point of Eq. (35).

The conclusion from the comparison (Figs. 4 and 5) is that the DSHE describes the reaction-diffusion problem almost quantitatively in the present case. In contrast, the CGLE fails completely (Figs. 2 and 3). So using the DSHE, one may reduce the numerical work to a small fraction (typically of the order 1:100) of that required for the corresponding direct integration of the reaction-diffusion equation. For the operating point considered, the behavior of the CGLE agrees with the fact that the coefficients α and β of the equation lie in a region where plane wave solutions are locally stable to long wave perturbations. This spurious stability is a consequence of the neglect of all dynamics out of the plane of oscillations. The correct behavior, as represented by the DSHE, can be explained by a stability analysis of plane wave solutions to the DSHE (27) which we have carried out using a modification of the approach described in [18]. We shall report these results in a separate paper.

Another reason for treating the particular reaction-diffusion system (35), in terms of the DSHE, Eq. (27), is the importance of the BZ-reaction, which it models. The BZ-reaction is perhaps the most studied nonlinear chemical reaction, and happens to have a very slow near-critical real mode almost everywhere in parameter space. (In fact, we have not found a fold-Hopf bifurcation anywhere in the model.) Furthermore, the slow real mode is very important to the dynamics, being associated with complex oscillations and chaos. So for a realistic treatment of a BZ-based reaction-diffusion system, the slow real mode cannot be neglected.

Recently, qualitative comparisons between solutions to the CGLE and experimentally observed spiral waves in the ferroin catalyzed BZ reaction were reported by Ouyang and Fleselles [21]. The ferroin catalyzed BZ reaction is not so well understood and characterized as the Ce^{4+} catalyzed version. Although a large part of the reactions involving bromomalonic acid are common for the two versions of the BZ system, reactions like the fifth of Eq. (34) do depend on the catalyst. Nevertheless, the possibility of slow real modes should be kept in mind, and the applicability of the CGLE cannot be taken for granted.

An advantage of the CGLE is that its coefficients α and β can be obtained directly from experiments [22] although the methods still need some refinement for higher accuracy. Unfortunately, measuring the coefficients of Eq. (27) is much more difficult. We may possibly get some progress using more general perturbation methods based on control theory, which we presently are developing. Otherwise one must work through optimized models of the

reaction considered.

In a case where several real modes are close to criticality, one must derive the appropriate amplitude equation from the general expression (19). This means calculating explicit expressions for the necessary coefficients as in Table 1. At the same time the linear equations for the coefficients of the amplitude transformation must be solved to the order desired. These steps are quite straightforward using software packages capable of performing symbolic manipulations such as Mathematica or Maple [23, 24]. Even though the multitude of coefficients to be calculated and equations to be solved grows rapidly with the number of slow modes, the gain in speed by using an amplitude equations may well make a solution feasible that in practice is impossible using the reaction-diffusion equation directly.

A Amplitude transformation

In [4], we derived an expression for the unfolded center manifold $W^c(\boldsymbol{\mu})$ in terms of coordinates y_i of $\mathbf{y} \in E^c$ in a basis of critical eigenvectors \mathbf{u}_i , namely

$$\mathbf{x} = \mathbf{y} + \mathbf{h}(\mathbf{y}, \boldsymbol{\mu}) = \sum_{i=1}^r y_i \mathbf{u}_i + \sum_{\mathbf{p}\mathbf{q}} \mathbf{h}_{\mathbf{p}\mathbf{q}} \mathbf{y}^{\mathbf{p}} \boldsymbol{\mu}^{\mathbf{q}} \quad (44)$$

in which $\mathbf{y}^{\mathbf{p}} = \prod_i y_i^{p_i}$ and $\boldsymbol{\mu}^{\mathbf{q}} = \prod_k \mu_k^{q_k}$. The coefficient vectors $\mathbf{h}_{\mathbf{p}\mathbf{q}}$ are solutions to the linear equations

$$\left(\mathbf{J} - \sum_{j=1}^r p_j \lambda_j \mathbf{I} \right) \cdot \mathbf{h}_{\mathbf{p}\mathbf{q}} = -\mathbf{Q}_{\mathbf{p}} \cdot \boldsymbol{\Phi}_{\mathbf{p}\mathbf{q}}, \quad (45a)$$

$$\mathbf{R}_{\mathbf{p}} \cdot \mathbf{h}_{\mathbf{p}\mathbf{q}} = \mathbf{0}. \quad (45b)$$

in which \mathbf{I} is the unit tensor, $\mathbf{R}_{\mathbf{p}}$ projects onto the resonant subspace and $\mathbf{Q}_{\mathbf{p}}$ removes the resonant components of any vector \mathbf{x} :

$$\mathbf{R}_{\mathbf{p}} \cdot \mathbf{x} = (\mathbf{I} - \mathbf{Q}_{\mathbf{p}}) \cdot \mathbf{x} = \sum_i (\mathbf{u}_i^* \cdot \mathbf{x}) \mathbf{u}_i. \quad (46)$$

The sum in Eq. (46) is taken over all components i for which the resonance condition (16) is satisfied (for a given order \mathbf{p}). The ‘‘source term’’ $\boldsymbol{\Phi}_{\mathbf{p}\mathbf{q}}$ on the right-hand side of Eq. (46) is given by the expression

$$\boldsymbol{\Phi}_{\mathbf{p}\mathbf{q}} = \mathbf{f}_{\mathbf{p}\mathbf{q}} - \sum_{\mathbf{p}'\mathbf{q}'} \mathbf{h}_{\mathbf{p}'\mathbf{q}'} \sum_{j=1}^r p'_j \mathbf{u}_j^* \cdot \mathbf{g}_{(\mathbf{p}-\mathbf{p}'+\delta_j)(\mathbf{q}-\mathbf{q}')}. \quad (47)$$

in terms of $\mathbf{f}_{\mathbf{p}\mathbf{q}}$ and lower order coefficients $\mathbf{h}_{\mathbf{p}'\mathbf{q}'}$ and $\mathbf{g}_{\mathbf{p}''\mathbf{q}''}$, given by

$$\mathbf{u}_j^* \cdot \mathbf{g}_{\mathbf{p}''\mathbf{q}''} = \begin{cases} \mathbf{u}_j^* \cdot \mathbf{f}_{\mathbf{p}''\mathbf{q}''} & \text{if } \mathbf{p}'' \cdot \boldsymbol{\lambda} = \lambda_j, \\ 0 & \text{otherwise.} \end{cases} \quad (48)$$

The vectors $\mathbf{f}_{\mathbf{p}\mathbf{q}}$ are coefficients in an expansion of the vector field $\mathbf{f}(\mathbf{x}, \boldsymbol{\mu})$ on the unfolded center manifold $W^c(\boldsymbol{\mu})$,

$$\mathbf{f}(\mathbf{y} + \mathbf{h}(\mathbf{y}, \boldsymbol{\mu}), \boldsymbol{\mu}) = \sum_{\mathbf{p}\mathbf{q}} \mathbf{f}_{\mathbf{p}\mathbf{q}} \mathbf{y}^{\mathbf{p}} \boldsymbol{\mu}^{\mathbf{q}}. \quad (49)$$

In practice, this expansion is obtained by substituting the expansion (44) in a Taylor expansion of $\mathbf{f}(\mathbf{x}, \boldsymbol{\mu})$ in terms of the usual multilinear forms, *e.g.*

$$\begin{aligned} \mathbf{F}_{\mathbf{xx}}(\mathbf{x}, \mathbf{x}) &= \sum_{i,j=1}^n \frac{\partial^2 \mathbf{F}}{\partial x_i \partial x_j} x_i x_j, & \mathbf{F}_{\mathbf{xxx}}(\mathbf{x}, \mathbf{x}, \mathbf{x}) &= \sum_{i,j,k=1}^n \frac{\partial^3 \mathbf{F}}{\partial x_i \partial x_j \partial x_k} x_i x_j x_k, \\ \mathbf{F}_{\boldsymbol{\mu}} \cdot \boldsymbol{\mu} &= \sum_{i=1}^s \frac{\partial \mathbf{F}}{\partial \mu_i} \mu_i, & \mathbf{F}_{\mathbf{x}\boldsymbol{\mu}}(\mathbf{x}, \boldsymbol{\mu}) &= \sum_{i=1}^n \sum_{j=1}^s \frac{\partial^2 \mathbf{F}}{\partial x_i \partial \mu_j} x_i \mu_j, \quad \text{etc.} \end{aligned} \quad (50)$$

Any coefficient $\mathbf{f}_{\mathbf{p}\mathbf{q}}$ of the expansion (49) is then obtained as an expression that may involve coefficients $\mathbf{h}_{\mathbf{p}'\mathbf{q}'}$. The important point now is that only lower orders (\mathbf{p}' , \mathbf{q}') appear for $\mathbf{h}_{\mathbf{p}'\mathbf{q}'}$ in $\mathbf{f}_{\mathbf{p}\mathbf{q}}$. So it is always possible to solve Eqs. (45)–(47) order by order.

As a result, the amplitude transformation (44) is obtained explicitly. This procedure provides a particular representation of the unfolded center manifold $W^c(\boldsymbol{\mu})$ in terms of the amplitudes y_i . Some simple examples of the calculation of the coefficients $\mathbf{f}_{\mathbf{p}\mathbf{q}}$ and explicit solutions of the linear equation (45) can be found in [4].

B Proof of Eqs. (12) and (13)

We use the expansion in Eq. (44) for $\mathbf{h}(\mathbf{y}, \boldsymbol{\mu})$ together with Eq. (14). For the left-hand side of Eq. (12), we then get

$$\sum_{\mathbf{p}\mathbf{q}} \mathbf{u}_i^* \cdot \mathbf{h}_{\mathbf{p}\mathbf{q}} \mathbf{z}^{\mathbf{p}} \boldsymbol{\mu}^{\mathbf{q}} \sum_{j=1}^r \frac{p_j}{z_j} \frac{\partial z_j}{\partial \tau} \frac{1}{T} \int_0^T e^{(\mathbf{p} \cdot \boldsymbol{\lambda} - \lambda_i) \theta} d\theta. \quad (51)$$

Here a term of order (\mathbf{p}, \mathbf{q}) vanishes because of the integral over θ unless $\mathbf{p} \cdot \boldsymbol{\lambda} = \lambda_i$. So the sum contains resonant terms only, but each of these vanishes because resonant components of $\mathbf{h}_{\mathbf{p}\mathbf{q}}$ vanish, $\mathbf{u}_i^* \cdot \mathbf{h}_{\mathbf{p}\mathbf{q}} = 0$, as Eq. (44) and Eq. (45) show. This demonstrates the identity in Eq. (12).

For Eq. (13), we use Eq. (44) and first observe that

$$\mathbf{J} \cdot \mathbf{y} - \frac{\partial \mathbf{y}}{\partial \theta} = \mathbf{J} \cdot e^{\mathbf{J}\theta} \cdot \mathbf{z} - \frac{\partial}{\partial \theta} (e^{\mathbf{J}\theta} \cdot \mathbf{z}) = 0 \quad (52)$$

From the expansion (44) of the transformation $\mathbf{h}(\mathbf{y}, \boldsymbol{\mu})$, we therefore get from the left-hand side of Eq. (13)

$$\sum_{\mathbf{p}\mathbf{q}} \mathbf{u}_i^* \cdot (\mathbf{J} - \mathbf{p} \cdot \boldsymbol{\lambda}) \cdot \mathbf{h}_{\mathbf{p}\mathbf{q}} \mathbf{z}^{\mathbf{p}} \boldsymbol{\mu}^{\mathbf{q}} \frac{1}{T} \int_0^T e^{(\mathbf{p} \cdot \boldsymbol{\lambda} - \lambda_i) \theta} d\theta. \quad (53)$$

Here only resonant terms contribute to the sum because of the integral, but these also vanish since $\mathbf{u}_i^* \cdot (\mathbf{J} - \mathbf{p} \cdot \boldsymbol{\lambda}) = 0$. The whole sum is therefore identically zero, so Eq. (13) is proved.

C Relation to the CGLE

Comparison of the DSHE (27) with the CGLE Eq. (26) contains a subtlety, which we now discuss. Equation (27a) has the same form as Eq. (26) apart from the coupling term $g_1 w z$.

But the coefficients g_1 and g also differ. They are defined in Tables 1 and 2 by very similar expressions, namely

$$g_1 = \mathbf{u}^* \cdot \mathbf{F}_{\mathbf{xx}}(\mathbf{u}, \mathbf{h}_{1100}) + \mathbf{u}^* \cdot \mathbf{F}_{\mathbf{xx}}(\bar{\mathbf{u}}, \mathbf{h}_{2000}) + \frac{1}{2} \mathbf{u}^* \cdot \mathbf{F}_{\mathbf{xxx}}(\mathbf{u}, \mathbf{u}, \bar{\mathbf{u}}), \quad (54)$$

$$g = \mathbf{u}^* \cdot \mathbf{F}_{\mathbf{xx}}(\mathbf{u}, \mathbf{h}_{110}) + \mathbf{u}^* \cdot \mathbf{F}_{\mathbf{xx}}(\bar{\mathbf{u}}, \mathbf{h}_{200}) + \frac{1}{2} \mathbf{u}^* \cdot \mathbf{F}_{\mathbf{xxx}}(\mathbf{u}, \mathbf{u}, \bar{\mathbf{u}}), \quad (55)$$

which differ only by \mathbf{h}_{110} replacing \mathbf{h}_{1100} and \mathbf{h}_{200} replacing \mathbf{h}_{2000} . The latter pair are identical because they are unique solutions to identical linear equations. But $\mathbf{h}_{110} \neq \mathbf{h}_{1100}$ because $(p, q) = (1, 1, 0, 0)$ is resonant for the real mode in the fold-Hopf bifurcation, whereas $(p, q) = (1, 1, 0)$ is nonresonant in the Hopf bifurcation. So the two vector coefficients are defined through two slightly different linear equations:

$$-\mathbf{J} \cdot \mathbf{h}_{1100} = \mathbf{F}_{\mathbf{xx}}(\mathbf{u}, \bar{\mathbf{u}}) - c_0 \mathbf{v}, \quad (56)$$

$$-\mathbf{J} \cdot \mathbf{h}_{110} = \mathbf{F}_{\mathbf{xx}}(\mathbf{u}, \bar{\mathbf{u}}). \quad (57)$$

Here, c_0 is the coefficient of $|w|^2$ in Eq. (27b). The second term of Eq. (56) arises through the projection operator \mathbf{Q}_3 in Table 1.

The physical significance is the following. In the CGLE, effects of components of the vector field \mathbf{F} out of the plane of oscillation can only be taken into account through the amplitude transformation. In the DSHE, the dynamics of the slow mode is directly accounted for in the amplitude equation. Consequently, it does not appear in the amplitude transformation, and as a result, the coefficients g_1 and g are in fact quite different. Compare their numerical values for the chosen operating point of the 4D Oregonator exhibited in Tables 5 and 6. Here, it is interesting to note that using g_1 in place of g in the CGLE would place the equation well inside the region of absolute instability (see Fig. 1d).

However, this comparison of parameters is misleading, since it neglects the effect of the term $g_0 w z$. To illuminate the issue, we first find an explicit relation between \mathbf{h}_{1100} and \mathbf{h}_{110} from the difference between Eqs. (56) and (57),

$$\mathbf{J} \cdot (\mathbf{h}_{1100} - \mathbf{h}_{110}) = c_0 \mathbf{v}. \quad (58)$$

Since \mathbf{J} is nonsingular, the solution is

$$\mathbf{h}_{1100} - \mathbf{h}_{110} = c_0 \mathbf{J}^{-1} \cdot \mathbf{v} = \frac{c_0}{\lambda_0} \mathbf{v}. \quad (59)$$

We can then use this result to derive an explicit relation between g_1 and g . Solving Eq. (59) for \mathbf{h}_{1100} and substituting the result in Eq. (54), we get, using the bilinearity of $\mathbf{F}_{\mathbf{xx}}(\mathbf{u}, \mathbf{h}_{1100})$ and the identity $\mathbf{h}_{2000} = \mathbf{h}_{200}$:

$$g_1 = g + \frac{c_0}{\lambda_0} \mathbf{u}^* \cdot \mathbf{F}_{\mathbf{xx}}(\mathbf{u}, \mathbf{v}) = g + \frac{c_0}{\lambda_0} g_0. \quad (60)$$

We can get an indication of the effect of the term $g_0 w z$ by examining the artificial situation where z is constrained to be homogeneous and stationary, so

$$z = -\frac{c_0}{\lambda_0} |w|^2 \quad (61)$$

from Eq. (27b). Substitution of this result in Eq. (27a) then yields

$$\dot{w} = \sigma_1 \mu w + (g_1 - \frac{c_0}{\lambda_0}) |w|^2 w + d_w \nabla^2 w, \quad (62)$$

which reduces to the CGLE, exactly, when Eq. (60) and the identity $d_w = d$ are employed. Thus it is the variation of z with space and time—the dynamics of the slow mode—that causes the deviation from CGLE behavior, which of course is no surprise.

In practice, we regain CGLE behavior if λ_0 becomes sufficiently large and negative implying that g_1 and g almost coalesce (according to Eq. (60)) and the linear term $\lambda_0 z$ in (27b) ensures that $|z|$ and hence $|g_0 w z|$ never becomes large. The magnitude of λ_0 should be compared with $\mu \operatorname{Re}\{\sigma_1\}$ first of all, and a condition for using the CGLE is $|\lambda_0| \gg \mu \operatorname{Re}\{\sigma_1\}$.

References

- [1] Field R.J. and Noyes R.M., 1974, Oscillations in chemical systems IV. Limit cycle behavior in a model of a real chemical reaction, *J. Chem. Phys.* 60, 1877–1884.
- [2] Zhabotinsky A.M., 1991, A history of chemical oscillations and waves, *Chaos* 1, 379–386.
- [3] Wang J., Sørensen P.G. and Hynne F., 1995, Transient complex oscillations in the closed Belousov-Zhabotinsky reaction: Experimental and computational studies, *Z. Phys. Chem.* 192, 63–76.
- [4] Ipsen M., Hynne F. and Sørensen P.G., 1998, Systematic derivation of amplitude equations and normal forms for dynamical systems, *Chaos* 8, 834–852.
- [5] Field R.J., Körös E. and Noyes R.M., 1972, Oscillations in chemical systems. Thorough analysis of temporal oscillations in the bromate-cerium-malonic acid system, *J. Amer. Chem. Soc.* 94, 8649–8664.
- [6] Field R.J. and Försterling H.D., 1986, On the oxybromine chemistry rate constants with cerium ions in the Field-Körös-Noyes mechanism of the Belousov-Zhabotinsky reaction, *J. Phys. Chem.* 90, 5400.
- [7] Hynne F., Sørensen P.G. and Møller T., 1993, Complete optimization of models of the Belousov-Zhabotinsky reaction at a Hopf bifurcation, *J. Chem. Phys.* 98, 219–230.
- [8] Aranson I., Levine H. and Tsimring L., 1996, Spiral competition in three-component excitable media, *Phys. Rev. Lett.* 76, 1170–1173.
- [9] FitzHugh R., 1961, Impulses and physiological states in theoretical models of nerve membrane, *Biophys. J* 1, 445–466.
- [10] Nagumo J.S., Arimoto S. and Youshizawa S., 1962, An active pulse transmission line simulating nerve axon, *Proc. IRE* 50, 2061–2071.
- [11] Bohr T., Jensen M.H., Paladin G. and Vulpiani A., 1998, *Dynamical Systems Approach to Turbulence*, Cambridge Nonlinear Science Series (Cambridge University Press, Cambridge).
- [12] Kuramoto Y., 1984, *Chemical Oscillations, Waves, and Turbulence* (Springer-Verlag, Berlin).
- [13] Kuramoto Y. and Tsuzuki T., 1976, Persistent propagation of concentration waves in dissipative media far from thermal equilibrium, *Prog. Theor. Phys.* 55, 356.
- [14] Sivashinsky G.I., 1977, Nonlinear analysis of hydrodynamic instability in laminar flames. Part I. Derivation of basic equations, *Acta Astronautica* 4, 1177.
- [15] Cross M.C. and Hohenberg P.C., 1993, Pattern formation outside of equilibrium, *Rev. Mod. Phys.* 65, 851–1112.
- [16] Ipsen M., Hynne F. and Sørensen P.G., 1997, Amplitude equations and chemical reaction-diffusion systems, *Int. J. Bifurcation and Chaos* 7, 1539–1554.
- [17] Huber G., Alstrøm P. and Bohr T., 1992, Nucleation and transients at the onset of vortex turbulence, *Phys. Rev. Lett* 69, 2380–2383.

- [18] Aranson I.S., Aranson L., Kramer L. and Weber A., 1992, Stability limits of spirals and travelling waves in nonequilibrium media, *Phys. Rev. A.* 46, R2992–R2995.
- [19] Aranson I.S., Golomb D. and Sompolinsky D., 1992, Spatial coherence and temporal chaos in macroscopic systems with asymmetrical couplings, *Phys. Rev. Lett.* 68, 3495–3498.
- [20] Ipsen M. and Schreiber I., 1998, Numerical determination of dynamical properties near hopf bifurcation points, preprint.
- [21] Ouyang Q. and Flesselles J.M., 1996, Transition from spirals to defect turbulence driven by a convective instability, *Nature* 379, 143–146.
- [22] Hynne F. and Sørensen P.G., 1993, Experimental determination of Ginzburg-Landau parameters for reaction-diffusion systems, *Phys. Rev. E* 48, 4106–4109.
- [23] Wolfram S., 1996, *The Mathematica Book* (Cambridge University Press, Cambridge, UK), third edn.
- [24] Monagan M.B., Geddes K.O., Heal K.M., Labahn G. and Vorkoetter S., 1996, *Maple V Programming Guide* (Springer-Verlag, New York).
- [25] Schwarzenbach R.P., Gschwend P.M. and Imboden D.H., 1993, *Environmental Organic Chemistry* (John Wiley & Sons, Inc, New York).

Captions of tables and figures

Figure 1: (a): Bifurcation diagram showing the locations of supercritical Hopf bifurcations in the 4D Oregonator model in the plane of the two parameters $[\text{BrO}_3^-]$ and $[\text{H}^+]$. (b): Variation of the dimensionless diffusion parameter α along the bifurcation curve in (a), plotted as a function of the parameter $[\text{BrO}_3^-]$. (c): Variation of the dimensionless parameter β along the branches in (a) plotted as a function of the parameter $[\text{BrO}_3^-]$. (d): Projections of the curves in (b) and (c) onto the (α, β) -plane together with the curves corresponding to the Eckhaus (EH) and absolute instability (AI) curves respectively. The Benjamin-Feir instability line (BF) is also shown.

Figure 2: Solution to the 4D Oregonator PDE at a finite distance from the bifurcation corresponding to an amplitude, which is 7.5% of the value of the stationary Ce^{4+} concentration. The three rows show the amplitude $|w|$ and two selected concentrations at the times shown below each column. Integrations were made on a 256×256 grid with no-flux boundary conditions and physical dimensions 4 cm in both directions.

Figure 3: Solution to the CGLE corresponding to the one for the 4D Oregonator shown in Fig. 2. The number below each column shows the time elapsed for that particular state. Integrations were made on a 256×256 grid with no-flux boundary conditions and physical dimensions 4 cm in both directions. The relative variation of $[\text{BrMA}]$ is extremely small (compare with Table 7). It is represented correctly by the colors but cannot be distinguished on the corresponding colorscale.

Figure 4: Solution to the 4D Oregonator PDE at a finite distance from the bifurcation point corresponding to an amplitude, 7.5% of the value of the stationary Ce^{4+} concentration. The number below each column shows the time elapsed for that particular state. The solution is the same as in Fig. 2, but the amplitude z is exhibited instead of $|w|$. Integrations were made on a 256×256 grid with no-flux boundary conditions and physical dimensions 4 cm in both directions.

Figure 5: Solution to the DSHE corresponding to that for the 4D Oregonator shown in Fig. 4. The number below each column shows the time elapsed for that particular state. Integrations were made on a 256×256 grid with no-flux boundary conditions and physical dimensions 4 cm in both directions.

Figure 6: Time series showing the local variation of $\text{Re } w$ (top) and z (bottom) at a particular grid point in the course of the pattern development shown in Fig. 5. Observe that the time variation of z is much slower than for $\text{Re } w$.

Figure 7: (a): Solution to Eq. (42) approaching the stable focus (r_s, z_s) .

Table 1: Formulas for calculating the coefficients of the amplitude transformation and amplitude equation for the fold-Hopf bifurcation. At the bifurcation, the Jacobian \mathbf{J} has three eigenvectors \mathbf{u} , $\bar{\mathbf{u}}$, and \mathbf{v} and left eigenvectors \mathbf{u}^* , $\bar{\mathbf{u}}^*$, and \mathbf{v}^* corresponding to the three critical eigenvalues $\lambda_1 = \bar{\lambda}_2 = i\omega_0$ and $\lambda_3 = 0$. The amplitude transformation $\mathbf{x} = \mathbf{y} + \mathbf{h}(\mathbf{y}, \mu)$, $\mathbf{y} = \mathbf{u}w e^{i\omega_0 t} + \text{c.c.} + \mathbf{v}z$, transforms a solution $w(\mathbf{r}, t), z(\mathbf{r}, t)$ of the amplitude equation to the motion $\mathbf{x}(\mathbf{r}, t)$ on the unfolded center manifold for the dynamical system. The vector coefficients \mathbf{h}_{pqrs} are determined as solutions to the linear equations indicated, in terms of the derivatives of the vector field \mathbf{F} . The coefficients of the amplitude equation can then be found through the explicit expressions indicated, in terms of the derivatives of \mathbf{F} and \mathbf{h}_{pqrs} . For any $\mathbf{x} \in \mathbb{R}^n$, the projections \mathbf{Q}_1 and \mathbf{Q}_3 are defined as $\mathbf{Q}_1 \cdot \mathbf{x} = \mathbf{x} - (\mathbf{u}^* \cdot \mathbf{x})\mathbf{u}$ and $\mathbf{Q}_3 \cdot \mathbf{x} = \mathbf{x} - (\mathbf{v}^* \cdot \mathbf{x})\mathbf{v}$ respectively.

Table 2: Formulas for calculating the coefficients of the amplitude transformation and amplitude equation for the Hopf bifurcation. At the bifurcation, the Jacobian \mathbf{J} has two complex conjugate eigenvectors \mathbf{u} and $\bar{\mathbf{u}}$ and left eigenvectors \mathbf{u}^* and $\bar{\mathbf{u}}^*$ corresponding to critical eigenvalues $\lambda_1 = \bar{\lambda}_2 = i\omega_0$. The amplitude transformation $\mathbf{x} = \mathbf{y} + \mathbf{h}(\mathbf{y}, \mu)$, $\mathbf{y} = \mathbf{u}we^{i\omega_0 t} + \text{c.c.}$, transforms a solution $w(\mathbf{r}, t)$ of the amplitude equation to the motion $\mathbf{x}(\mathbf{r}, t)$ on the unfolded center manifold for the dynamical system. The vector coefficients $\mathbf{h}_{pq\mathbf{s}}$ are determined as solutions to the linear equations indicated, in terms of the derivatives of the vector field \mathbf{F} . The coefficients of the amplitude equation can then be found through the explicit expressions indicated, in terms of the derivatives of \mathbf{F} and $\mathbf{h}_{pq\mathbf{s}}$. For any $\mathbf{x} \in \mathbb{R}^n$, the projection \mathbf{Q}_1 is defined as $\mathbf{Q}_1 \cdot \mathbf{x} = \mathbf{x} - (\mathbf{u}^* \cdot \mathbf{x})\mathbf{u}$.

Table 3: Rate constants k_1, \dots, k_7 , constant malonic acid concentration M , and diffusion constants D_X, D_Y, D_Z , and D_U used for numerical simulations for the 4D Oregonator reaction-diffusion equation (35). The values of the rate constants are based on [3] but have been modified slightly in the calculations presented here. Diffusion constants D_X, \dots, D_Z are from [22], whereas the value of D_U was estimated by an interpolation scheme described in [25, p. 196].

Table 4: Hopf bifurcation point for the 4D Oregonator used as a reference for the operating point actually used in the calculations. The table shows the parameters, the stationary point, and the eigenvalues $\pm i\omega_0$, λ_3 , and λ_4 of the Jacobian matrix at that point.

Table 5: Ginzburg-Landau parameters at the Hopf bifurcation, Table 4, for the 4D Oregonator Eq. (35) with parameters shown in Table 3.

Table 6: Coefficients for the distributed slow-Hopf equation (27) at the Hopf bifurcation, Table 4, for the 4D Oregonator Eq. (35) with parameters shown in Table 3.

Table 7: Left and right eigenvectors of the Jacobian matrix at the Hopf bifurcation, Table 4, for the 4D Oregonator Eq. (35) with parameters shown in Table 3. The eigenvectors \mathbf{u}^* (left) and \mathbf{v} (right) correspond to eigenvalues $i\omega_0$ and λ_3 respectively. They illuminate the special role played by BrMA in the 4D Oregonator.

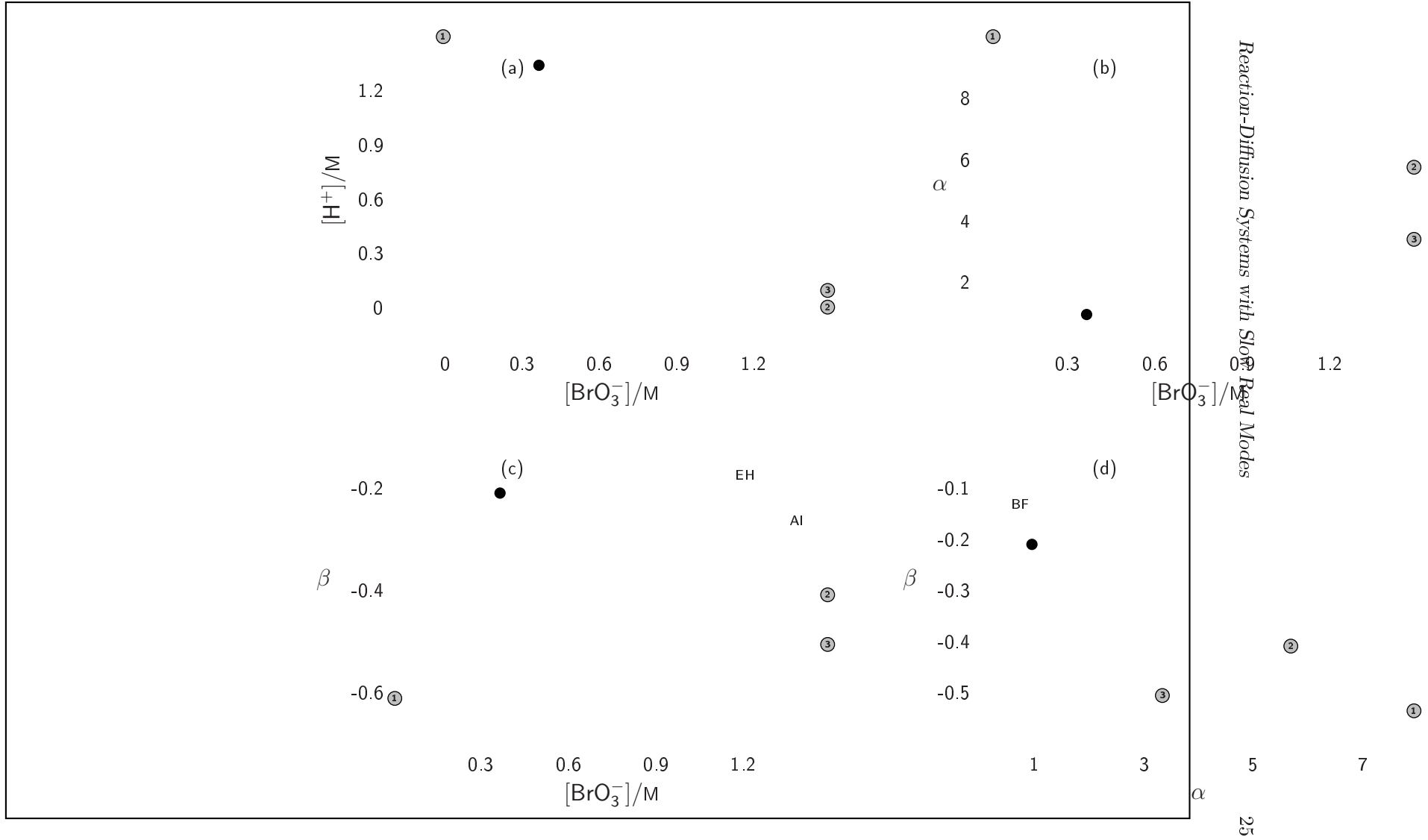


Figure 1:

Figure 2:

Figure 3:

Figure 4:

Figure 5:

Figure 6:

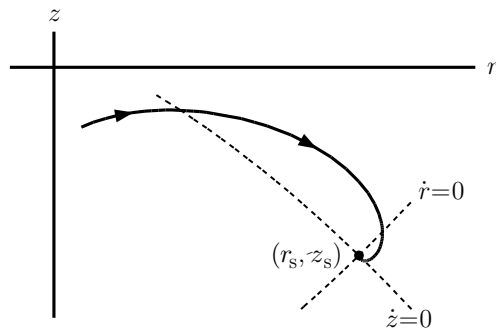


Figure 7:

<i>Fold-Hopf Bifurcation</i>	
Transformation $\mathbf{x} = \mathbf{y} + \mathbf{h}(\mathbf{y}, \mu)$	$\mathbf{x} = \mathbf{u}\psi + \overline{\mathbf{u}}\overline{\psi} + \mathbf{v}z + \mathbf{h}_{2000}\psi^2 + \mathbf{h}_{1100} \psi ^2 + \mathbf{h}_{0200}\overline{\psi}^2 + \mathbf{h}_{0020}z^2 + \mathbf{h}_{1010}\psi z + \mathbf{h}_{0110}\overline{\psi}z +$ $\mathbf{h}_{3000}\psi^3 + \mathbf{h}_{2100} \psi ^2\psi + \mathbf{h}_{1200} \psi ^2\overline{\psi} + \mathbf{h}_{0300}\overline{\psi}^3 + \mathbf{h}_{0030}z^3 + \mathbf{h}_{2010}\psi^2z + \mathbf{h}_{1110} \psi ^2z +$ $\mathbf{h}_{0210}\overline{\psi}^2z + \mathbf{h}_{1020}\psi z^2 + \mathbf{h}_{0120}\overline{\psi}z^2 + (\mathbf{h}_{0001} + \mathbf{h}_{1001}\psi + \mathbf{h}_{0101}\overline{\psi} + \mathbf{h}_{0011}z)\mu, \quad \psi = w e^{i\omega_0 t}$
Second order	<i>Linear equations for \mathbf{h}_{pqrs}</i>
w^2	$-(\mathbf{J} - 2i\omega_0\mathbf{I}) \cdot \mathbf{h}_{2000} = \frac{1}{2}\mathbf{F}_{\mathbf{xx}}(\mathbf{u}, \mathbf{u}) \quad \mathbf{h}_{0200} = \overline{\mathbf{h}}_{2000}$
$ w ^2$	$-\mathbf{J} \cdot \mathbf{h}_{1100} = -\mathbf{Q}_3 \cdot \mathbf{F}_{\mathbf{xx}}(\mathbf{u}, \overline{\mathbf{u}})$
wz	$-(\mathbf{J} - i\omega_0\mathbf{I}) \cdot \mathbf{h}_{1010} = \mathbf{Q}_1 \cdot \mathbf{F}_{\mathbf{xx}}(\mathbf{u}, \mathbf{v}) \quad \mathbf{u}^* \cdot \mathbf{h}_{0020} = 0 \quad \mathbf{h}_{0110} = \overline{\mathbf{h}}_{1010}$
z^2	$-\mathbf{J} \cdot \mathbf{h}_{0020} = \frac{1}{2}\mathbf{Q}_3 \cdot \mathbf{F}_{\mathbf{xx}}(\mathbf{v}, \mathbf{v}) \quad \mathbf{v}^* \cdot \mathbf{h}_{0020} = 0$
Third order	<i>Linear equations for \mathbf{h}_{pqrs}</i>
w^3	$-(\mathbf{J} - 3i\omega_0\mathbf{I}) \cdot \mathbf{h}_{3000} = \mathbf{F}_{\mathbf{xx}}(\mathbf{u}, \mathbf{h}_{2000}) + \frac{1}{6}\mathbf{F}_{\mathbf{xxx}}(\mathbf{u}, \mathbf{u}, \mathbf{u}) \quad \mathbf{h}_{0300} = \overline{\mathbf{h}}_{3000}$
$ w ^2w$	$-(\mathbf{J} - i\omega_0\mathbf{I}) \cdot \mathbf{h}_{2100} = \mathbf{Q}_1 \cdot (\mathbf{F}_{\mathbf{xx}}(\mathbf{u}, \mathbf{h}_{1100}) + \mathbf{F}_{\mathbf{xx}}(\overline{\mathbf{u}}, \mathbf{h}_{2000}) + \frac{1}{2}\mathbf{F}_{\mathbf{xxx}}(\mathbf{u}, \mathbf{u}, \overline{\mathbf{u}})) \quad \mathbf{u}^* \cdot \mathbf{h}_{2100} = 0 \quad \mathbf{h}_{1200} = \overline{\mathbf{h}}_{2100}$
wz^2	$-(\mathbf{J} - i\omega_0\mathbf{I}) \cdot \mathbf{h}_{1020} = \mathbf{Q}_1 \cdot (\mathbf{F}_{\mathbf{xx}}(\mathbf{u}, \mathbf{h}_{0020}) + \mathbf{F}_{\mathbf{xx}}(\mathbf{v}, \mathbf{h}_{1010}) + \frac{1}{2}\mathbf{F}_{\mathbf{xxx}}(\mathbf{u}, \mathbf{v}, \mathbf{v})) \quad \mathbf{h}_{0120} = \overline{\mathbf{h}}_{1020}$
$ w ^2z$	$-\mathbf{J} \cdot \mathbf{h}_{1110} = \mathbf{Q}_3 \cdot (\mathbf{F}_{\mathbf{xx}}(\mathbf{u}, \mathbf{h}_{0110}) + \mathbf{F}_{\mathbf{xx}}(\overline{\mathbf{u}}, \mathbf{h}_{1010}) + \mathbf{F}_{\mathbf{xx}}(\mathbf{v}, \mathbf{h}_{1100}) + \mathbf{F}_{\mathbf{xxx}}(\mathbf{u}, \overline{\mathbf{u}}, \mathbf{v}))$
w^2z	$-(\mathbf{J} - 2i\omega_0\mathbf{I}) \cdot \mathbf{h}_{2010} = \mathbf{F}_{\mathbf{xx}}(\mathbf{u}, \mathbf{h}_{1010}) + \mathbf{F}_{\mathbf{xx}}(\mathbf{v}, \mathbf{h}_{2000}) + \frac{1}{2}\mathbf{F}_{\mathbf{xxx}}(\mathbf{u}, \mathbf{u}, \mathbf{v}) - g_2\mathbf{h}_{2000} \quad \mathbf{h}_{0210} = \overline{\mathbf{h}}_{2010}$
z^3	$-\mathbf{J} \cdot \mathbf{h}_{0030} = \mathbf{Q}_3 \cdot (\mathbf{F}_{\mathbf{xx}}(\mathbf{v}, \mathbf{h}_{0020}) + \frac{1}{6}\mathbf{F}_{\mathbf{xxx}}(\mathbf{v}, \mathbf{v}, \mathbf{v})) \quad \mathbf{v}^* \cdot \mathbf{h}_{0030} = 0$
Unfoldings	<i>Linear equations for \mathbf{h}_{pqrs}</i>
μ	$-\mathbf{J} \cdot \mathbf{h}_{0001} = \mathbf{Q}_3 \cdot \mathbf{F}_\mu \quad \mathbf{v}^* \cdot \mathbf{h}_{0001} = 0$
μw	$-(\mathbf{J} - i\omega_0\mathbf{I}) \cdot \mathbf{h}_{1001} = \mathbf{Q}_1 \cdot (\mathbf{F}_{\mathbf{x}\mu} \cdot \mathbf{u} + \mathbf{F}_{\mathbf{xx}}(\mathbf{u}, \mathbf{h}_{0001})) \quad \mathbf{u}^* \cdot \mathbf{h}_{1001} = 0 \quad \mathbf{h}_{0101} = \overline{\mathbf{h}}_{1001}$
μz	$-\mathbf{J} \cdot \mathbf{h}_{0011} = \mathbf{Q}_3 \cdot (\mathbf{F}_{\mathbf{x}\mu} \cdot \mathbf{v} + \mathbf{F}_{\mathbf{xx}}(\mathbf{v}, \mathbf{h}_{0001})) \quad \mathbf{v}^* \cdot \mathbf{h}_{0011} = 0$
Amplitude equation	$\dot{w} = \sigma_1\mu w + g_0wz + g_1 w ^2w + g_2wz^2 + d_w\nabla^2w, \quad d_w = \mathbf{u}^* \cdot \mathbf{D} \cdot \mathbf{u}, \quad d_z = \mathbf{v}^* \cdot \mathbf{D} \cdot \mathbf{v}$ $\dot{z} = \rho_0\mu + c_0 w ^2 + c_1z^2 + c_2 w ^2z + c_3z^3 + d_z\nabla^2z.$
Resonant coefficients	$g_0 = \mathbf{u}^* \cdot \mathbf{F}_{\mathbf{xx}}(\mathbf{u}, \mathbf{v})$ $g_1 = \mathbf{u}^* \cdot \mathbf{F}_{\mathbf{xx}}(\mathbf{u}, \mathbf{h}_{1100}) + \mathbf{u}^* \cdot \mathbf{F}_{\mathbf{xx}}(\overline{\mathbf{u}}, \mathbf{h}_{2000}) + \frac{1}{2}\mathbf{u}^* \cdot \mathbf{F}_{\mathbf{xxx}}(\mathbf{u}, \mathbf{u}, \overline{\mathbf{u}})$ $g_2 = \mathbf{u}^* \cdot \mathbf{F}_{\mathbf{xx}}(\mathbf{u}, \mathbf{h}_{0020}) + \mathbf{u}^* \cdot \mathbf{F}_{\mathbf{xx}}(\mathbf{v}, \mathbf{h}_{1010}) + \frac{1}{2}\mathbf{u}^* \cdot \mathbf{F}_{\mathbf{xxx}}(\mathbf{u}, \mathbf{v}, \mathbf{v})$ $c_0 = \mathbf{v}^* \cdot \mathbf{F}_{\mathbf{xx}}(\mathbf{u}, \overline{\mathbf{u}}), \quad c_1 = \frac{1}{2}\mathbf{v}^* \cdot \mathbf{F}_{\mathbf{xx}}(\mathbf{v}, \mathbf{v})$ $c_2 = \mathbf{v}^* \cdot \mathbf{F}_{\mathbf{xx}}(\mathbf{u}, \mathbf{h}_{0110}) + \mathbf{v}^* \cdot \mathbf{F}_{\mathbf{xx}}(\overline{\mathbf{u}}, \mathbf{h}_{1010}) + \mathbf{v}^* \cdot \mathbf{F}_{\mathbf{xx}}(\mathbf{v}, \mathbf{h}_{1100}) + \mathbf{v}^* \cdot \mathbf{F}_{\mathbf{xxx}}(\mathbf{u}, \overline{\mathbf{u}}, \mathbf{v})$ $c_3 = \mathbf{v}^* \cdot \mathbf{F}_{\mathbf{xx}}(\mathbf{v}, \mathbf{h}_{0020}) + \frac{1}{6}\mathbf{v}^* \cdot \mathbf{F}_{\mathbf{xxx}}(\mathbf{v}, \mathbf{v}, \mathbf{v})$ $\sigma_1 = \mathbf{u}^* \cdot \mathbf{F}_{\mathbf{x}\mu} \cdot \mathbf{u} + \mathbf{u}^* \cdot \mathbf{F}_{\mathbf{xx}}(\mathbf{u}, \mathbf{h}_{0001}), \quad \rho_0 = \mathbf{v}^* \cdot \mathbf{F}_\mu$

Table 1:

<i>Hopf Bifurcation</i>		
Transformation $\mathbf{x} = \mathbf{y} + \mathbf{h}(\mathbf{y}, \mu)$	$\mathbf{x} = \mathbf{u}\psi + \bar{\mathbf{u}}\bar{\psi} + \mathbf{h}_{200}\psi^2 + \mathbf{h}_{110} \psi ^2 + \mathbf{h}_{020}\bar{\psi}^2 + \mathbf{h}_{300}\psi^3 + \mathbf{h}_{210} \psi ^2\psi + \mathbf{h}_{120} \psi ^2\bar{\psi} + \mathbf{h}_{030}\bar{\psi}^3 + \mathbf{h}_{001}\mu + (\mathbf{h}_{101}\psi + \mathbf{h}_{011}\bar{\psi})\mu,$	$\psi = we^{i\omega_0 t}$
<i>Second order</i>		
	<i>Linear equations for \mathbf{h}_{pqs}</i>	
w^2	$-(\mathbf{J} - 2i\omega_0\mathbf{I}) \cdot \mathbf{h}_{200} = \frac{1}{2}\mathbf{F}_{\mathbf{xx}}(\mathbf{u}, \mathbf{u})$	$\mathbf{h}_{020} = \bar{\mathbf{h}}_{200}$
$ w ^2$	$-\mathbf{J} \cdot \mathbf{h}_{110} = \mathbf{F}_{\mathbf{xx}}(\mathbf{u}, \bar{\mathbf{u}})$	
<i>third order</i>		
	<i>Linear equations for \mathbf{h}_{pqs}</i>	
w^3	$-(\mathbf{J} - 3i\omega_0\mathbf{I}) \cdot \mathbf{h}_{300} = \mathbf{F}_{\mathbf{xx}}(\mathbf{u}, \mathbf{h}_{200}) + \frac{1}{6}\mathbf{F}_{\mathbf{xxx}}(\mathbf{u}, \mathbf{u}, \mathbf{u})$	$\mathbf{h}_{030} = \bar{\mathbf{h}}_{300}$
$ w ^2 w$	$-(\mathbf{J} - i\omega_0\mathbf{I}) \cdot \mathbf{h}_{210} = \mathbf{Q}_1 \cdot (\mathbf{F}_{\mathbf{xx}}(\mathbf{u}, \mathbf{h}_{110}) + \mathbf{F}_{\mathbf{xx}}(\bar{\mathbf{u}}, \mathbf{h}_{200}) + \frac{1}{2}\mathbf{F}_{\mathbf{xxx}}(\mathbf{u}, \mathbf{u}, \bar{\mathbf{u}}))$	$\mathbf{u}^* \cdot \mathbf{h}_{210} = 0 \quad \mathbf{h}_{120} = \bar{\mathbf{h}}_{210}$
<i>Unfoldings</i>		
	<i>Linear equations for \mathbf{h}_{pqs}</i>	
μ	$-\mathbf{J} \cdot \mathbf{h}_{001} = \mathbf{F}_\mu$	
μw	$-(\mathbf{J} - i\omega_0\mathbf{I}) \cdot \mathbf{h}_{101} = \mathbf{Q}_1 \cdot (\mathbf{F}_{\mathbf{x}\mu} \cdot \mathbf{u} + \mathbf{F}_{\mathbf{xx}}(\mathbf{u}, \mathbf{h}_{001}))$	$\mathbf{u}^* \cdot \mathbf{h}_{101} = 0 \quad \mathbf{h}_{011} = \bar{\mathbf{h}}_{101}$
Amplitude equation	$\dot{w} = \sigma_1 \mu w + g w ^2 w + d\nabla^2 w$	$d = \mathbf{u}^* \cdot \mathbf{D} \cdot \mathbf{u}$
Resonant coefficients	$g = \mathbf{u}^* \cdot \mathbf{F}_{\mathbf{xx}}(\mathbf{u}, \mathbf{h}_{110}) + \mathbf{u}^* \cdot \mathbf{F}_{\mathbf{xx}}(\bar{\mathbf{u}}, \mathbf{h}_{200}) + \frac{1}{2}\mathbf{u}^* \cdot \mathbf{F}_{\mathbf{xxx}}(\mathbf{u}, \mathbf{u}, \bar{\mathbf{u}})$ $\sigma_1 = \mathbf{u}^* \cdot \mathbf{F}_{\mathbf{x}\mu} \cdot \mathbf{u} + \mathbf{u}^* \cdot \mathbf{F}_{\mathbf{xx}}(\mathbf{u}, \mathbf{h}_{001})$	

Table 2:

<i>Constant</i>	<i>Value</i>	<i>Constant</i>	<i>Value</i>
$k_1/M^{-3}s^{-1}$	1.6	k_7/M^{-1}	0.0003
$k_2/M^{-2}s^{-1}$	2.5×10^6	M/M	0.44
$k_3/M^{-2}s^{-1}$	33.0	D_X/cm^2s^{-1}	1.0×10^{-5}
$k_4/M^{-1}s^{-1}$	3.0×10^3	D_Y/cm^2s^{-1}	1.6×10^{-5}
$k_5/M^{-1}s^{-1}$	30.0	D_Z/cm^2s^{-1}	0.6×10^{-5}
$k_6/M^{-2}s^{-1}$	0.18	D_U/cm^2s^{-1}	6.7×10^{-6}

Table 3:

<i>Parameter</i>	<i>Value</i>
$[\text{BrO}_3^-]_{\text{Hopf}}/\text{M}$	0.3662
$[\text{H}^+]_{\text{Hopf}}/\text{M}$	1.3416
$[\text{HBrO}]_0/\text{M}$	9.8679×10^{-7}
$[\text{Br}^-]_0/\text{M}$	7.0929×10^{-6}
$[\text{Ce}^{4+}]_0/\text{M}$	1.3185×10^{-5}
$[\text{BrMA}]_0/\text{M}$	7.8262×10^{-2}
ω_0/s^{-1}	2.1911
λ_3/s^{-1}	-3.0731×10^{-4}
λ_4/s^{-1}	-10.4379

Table 4:

<i>Parameter</i>	<i>Value</i>
σ_1/s^{-1}	$-2.57 + i1.14$
$g/10^{10} \text{M}^{-2}\text{s}^{-1}$	$2.19 + i2.09$
$d/10^{-5} \text{cm}^2\text{s}^{-1}$	$1.00 - i2.10$
α	0.96
β	-0.21

Table 5:

<i>Parameter</i>	<i>Value</i>
λ_0/s^{-1}	-3.07×10^{-4}
σ_1/s^{-1}	$-2.57 + i1.14$
$g_0/10^5 \text{M}^{-1}\text{s}^{-1}$	$0.64 + i1.00$
$g_1/10^{10} \text{M}^{-2}\text{s}^{-1}$	$1.09 + i3.80$
$c_0/10 \text{M}^{-1}\text{s}^{-1}$	-5.25
$d_w/10^{-5} \text{cm}^2\text{s}^{-1}$	$1.00 - i2.10$
$d_z/10^{-6} \text{cm}^2\text{s}^{-1}$	6.70

Table 6:

<i>Species</i>	$\text{Re } \mathbf{u}^*$	$\text{Im } \mathbf{u}^*$	\mathbf{v}
HBrO ₂	7.546×10^{-1}	-1.843	3.382×10^{-3}
Br ⁻	1.699×10^{-1}	8.390×10^{-1}	-1.138×10^{-2}
Ce ⁴⁺	4.665×10^{-1}	2.519×10^{-1}	1.0
BrMA	7.975×10^{-5}	4.032×10^{-5}	-5.857×10^3

Table 7: